



A STUDY OF THE THERMAL ENVIRONMENT DEVELOPED BY A TRAVELING  
SLIPPER AT HIGH VELOCITY

THESIS

Kathleen H. Le, Captain, USAF

AFIT-ENY-13-M-20

**DEPARTMENT OF THE AIR FORCE  
AIR UNIVERSITY**

***AIR FORCE INSTITUTE OF TECHNOLOGY***

---

**Wright-Patterson Air Force Base, Ohio**

APPROVED FOR PUBLIC RELEASE; DISTRIBUTION UNLIMITED.

The views expressed in this thesis are those of the author and do not reflect the official policy or position of the United States Air Force, Department of Defense, or the United States Government. This material is declared a work of the United States Government and is not subject to copyright protection in the United States.

AFIT-ENY-13-M-20

A STUDY OF THE THERMAL ENVIRONMENT DEVELOPED BY A TRAVELING  
SLIPPER AT HIGH VELOCITY

THESIS

Presented to the Faculty

Department of Aeronautics and Astronautics

Graduate School of Engineering and Management

Air Force Institute of Technology

Air University

Air Education and Training Command

In Partial Fulfillment of the Requirements for the  
Degree of Master of Science in Aeronautical Engineering

Kathleen H. Le, B.S.

Captain, USAF

March 2013

APPROVED FOR PUBLIC RELEASE; DISTRIBUTION UNLIMITED.

AFIT-ENY-13-M-20

A STUDY OF THE THERMAL ENVIRONMENT DEVELOPED BY A TRAVELING  
SLIPPER AT HIGH VELOCITY

Kathleen H. Le, B.S.  
Captain, USAF

Approved:

\_\_\_\_\_  
Anthony N. Palazotto, Ph. D. (Chairman)

\_\_\_\_\_  
Date

\_\_\_\_\_  
William P. Baker, Ph. D. (Member)

\_\_\_\_\_  
Date

\_\_\_\_\_  
James L. Rutledge, Maj, USAF (Member)

\_\_\_\_\_  
Date

## **Abstract**

The research presented in this thesis is developed from the relative sliding motion of a traveling slipper and stationary rail at the Holloman High Speed Test Track located at Holloman AFB, NM. The high velocity condition of the slipper traveling down the rail creates a thermal environment that is of interest to the researchers at the Air Force Institute of Technology. The high temperatures coupled with high velocity leads to a non-linear problem known as melt wear. The goal of this research is to characterize the amount of heat flow going into the slipper as it traverses the rail and to predict the total melt wear of the slipper.

The heat transfer analysis of the Holloman event is carried out by considering one-dimensional heat conduction into the slipper due to frictional energy. The frictional energy is produced by the relative motion between the slipper and the rail. Energy in the form of heat translates to high temperatures which eventually reach the point of melt. The solution to how much melt wear is produced is found by considering the partition fraction of heat entering into the slipper. Different considerations for this partition fraction are presented in this work. One of the functions is based on a mathematical approach by considering a Gaussian distribution. This function provides a solution that gives the least amount of melt wear at 0.79%. It also assumes that the slipper is always in contact with the rail; however it is a physical reality that it bounces due to the aerodynamics and imperfections on the rail. Therefore, other partition functions are discussed that take the bouncing effect into account. The total melt wear predicted using the partition functions was found to be 2-3%. The outcome is heavily based on the partition function as it drives the prediction on the total melt wear.

## **Acknowledgments**

First and foremost, I thank my family for their support and encouragement while I pursued my graduate education at AFIT. My parents have shown tremendous love, patience, and generosity as I worked to finish my thesis. I could not have been successful without their encouragement on a daily basis.

I also thank my advisor Dr. Anthony Palazotto for his enduring effort to advance my education. His expertise in all areas has been invaluable to my research. He made every meeting worthwhile and spent much of his own time researching articles and developing theory that have helped my research in many ways. Throughout this journey Dr. Palazotto was there guiding me, and I am very grateful. I also thank Dr. William Baker for his expertise. He helped me tremendously in understanding the numerical intricacies of the melt wear problem. I am grateful for his passion and the enthusiasm he brought to every meeting. I also thank Maj Rutledge for being on my thesis committee. He provided a great wealth of knowledge in the heat transfer analysis and made great contributions to improving my thesis.

Kathleen H. Le

# Table of Contents

	Page
Abstract.....	iv
Acknowledgments.....	v
Table of Contents.....	vi
Nomenclature.....	viii
I. Introduction.....	1
1.1 Research Objective.....	1
1.2 Holloman AFB High Speed Test Track Background.....	2
1.3 Related Material to Test Track Thermal Analysis.....	4
II. Theory.....	7
2.1 Chapter Overview.....	7
2.2 Heat Transfer Equations.....	8
2.3 Wolfson Experiment.....	10
III. Methodology.....	13
3.1 Chapter Overview.....	13
3.2 Why Friction Matters.....	13
3.3 Heat Flux Boundary Conditions.....	18
3.4 Heat Equation with Melt Consideration.....	21
3.5 How the Melt Layer is Developed Numerically.....	23
3.5.1 Finite Difference Method.....	25
3.6 Understanding the MATLAB Code.....	30
IV. Analysis and Results.....	34
4.1 Wolfson Experiment Results.....	34
4.2 A More Physics-Based Approach to the Partition Function.....	55
V. Conclusions and Recommendations.....	69
5.1 Summary.....	69
5.2 Conclusions.....	69
5.3 Significance of Research.....	71
5.4 Recommendations for Future Research.....	72
Appendix A. DADS Data in MATLAB Code.....	73

A.1 MATLAB Code Description.....	73
A.2 DADS Data File Extraction MATLAB Code.....	73
Appendix B. Heat Transfer MATLAB Code.....	75
Bibliography .....	81

## Nomenclature

$a$	acceleration	$\text{m/s}^2$
$A$	slipper surface area	$\text{m}^2$
$d\sigma/dt$	rate of melt	$\text{m/s}$
$h$	convection coefficient	$\text{W/m}^2\cdot\text{K}$
$F_f$	frictional force	$\text{N}$
$l$	latent heat of fusion	$\text{J/kg}$
$k$	thermal conductivity	$\text{W/m}\cdot\text{K}$
$P$	pressure	$\text{Pa}$
$P_0$	constant pressure	$\text{Pa}$
$q$	rate of heat energy	$\text{W}$
$q''$	heat flux	$\text{W/m}^2$
$t$	time	$\text{s}$
$t_m$	melt time	$\text{s}$
$t_0$	initial time	$\text{s}$
$T$	temperature	$\text{K}$
$T_a$	ambient temperature	$\text{K}$
$T_s$	surface temperature	$\text{K}$
$T_\infty$	air temperature	$\text{K}$
$v$	velocity	$\text{m/s}$
$v_0$	constant velocity	$\text{m/s}$
$x$	distance into slipper	$\text{m}$

$\alpha$	partition function	
$\alpha_0$	initial partition	
$\alpha_m$	melt partition	
$\Delta\sigma$	melt depth	m
$\Delta t$	time increment	s
$\kappa$	thermal diffusivity	m <sup>2</sup> /s
$\mu$	coefficient of friction	
$\rho$	density	kg/m <sup>3</sup>
$\sigma$	melt layer	m
$\omega$	frequency	Hz

# A STUDY OF THE THERMAL ENVIRONMENT DEVELOPED BY A TRAVELING SLEIGH AT HIGH VELOCITY

## I. Introduction

The goal of this research is to study the melt wear phenomenon of sliding materials at high velocity. In particular, the Holloman High Speed Test Track (HHSTT) located at Holloman Air Force Base (AFB) is home to a 10-mile long test track in which the wear of steel slippers is being considered. This chapter will discuss the overall research objective, provide an overview of the HHSTT, and introduce previous research efforts in this area of study.

### 1.1 Research Objective

The evaluation of melting due to sliding has been carried out in several previous works. What makes this research different is the fact that the developed melt is a byproduct of high speed travel. The researchers at the Air Force Institute of Technology (AFIT) are interested in developing a model depicting the amount of material removed as a sled proceeds down the HHSTT located at Holloman AFB, NM. The work reported in this thesis is directed to the frictional energy developed by the relative velocity between a moving slipper and a stationary rail. This energy is delegated to the separation between the slipper and the rail via a partition function  $\alpha$ . The partition function is of particular interest in the present research. Various functions are developed in association with a finite difference approximation of heat flow with respect to time into the slipper. A solution is found which considers the heat conduction, the latent heat of fusion and the convective heat loss due to bounce. The HHSTT provided raw data called Dynamic

Analysis and Design Systems (DADS) from a January 2008 mission and included mission run time, position, velocity, and vertical slipper contact forces on the rail. The outcome of this research is utilizing this data to determine a total wear dimension within the slipper due to an experimental run from a January 2008 test. The objective of this research is developing the partition function that models the heat energy partitioned into the rail and slipper.

## **1.2 Holloman AFB High Speed Test Track Background**

The HHSTT in Figure 1.1 carries out a wide array of high velocity tests for the Department of Defense (DoD). These tests range from payloads up to full-scale aircraft testing at realistic flight velocities. Some of the advantages of utilizing the HHSTT include cost effectiveness, realistic flight conditions, early life-cycle risk reduction, and comprehensive data acquisition. The test track bridges the gap between laboratory experiments and full-scale flight tests. It is a test-like-you-fly capability for the DoD.



**Figure 1.1: 10-mile Long HHSTT**

The particular test layout considered is shown in Figure 1.2. It is comprised of four stages, three of which are pusher sleds that propel the fourth stage equipped with the test payload. The sled system shown in Figure 1.3 is from a world record test that was conducted on 30 April 2003 for the Missile Defense Agency (MDA). The test set a land speed record in which the sled obtained a velocity of 6,543 miles per hour while delivering a 192-pound payload onto the target. The sled system shown in Figure 1.2 rides along two rails made of 1080 steel. The sleds are held onto the track with “shoes” or “slippers” made from VascoMax (VM) 300 steel and shown in Figure 1.4

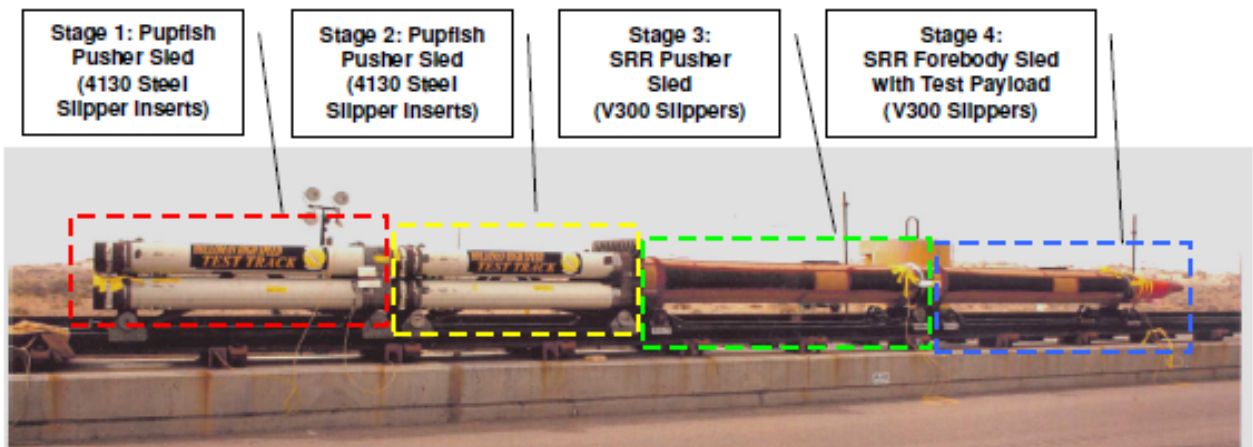


**Figure 1.2: Test Track Layout**



**Figure 1.3: Sled System**

The slipper shown is of particular interest to the HHSTT experimenters and researchers. It is the interface between the upper surface of the rail and the bottom of the slipper that relates the study of melt wear to this research.



**Figure 1.4: Slipper-Rail Interface**

### **1.3 Related Material to Test Track Thermal Analysis**

The consideration of temperature effects on the test track has been a topic of interest for many years. In previous works, researchers have examined the phenomenon

of gouging where nonlinear deformations occur between the slipper and rail interface due to high velocities. In 2002, Laird studied this effect and observed that gouging occurs when the rocket sled exceeds 1500 m/s and is caused by intermittent contact between the slipper and rail [6]. This intermittent contact is known as bouncing and is a factor in the thermal analysis described in this research. Laird also observed that gouging occurs under a combination of high bearing pressure and high temperature. This combination leads to the problem of melt wear. Melt wear is a difficult entity to predict due to the highly nonlinear effects of temperature.

In 2003, Laird considered the thermal environment to play a large factor in gouging. He noted that the heating of materials changes their material properties, including lowering the yield strength [7]. Until this time, gouging had only been considered at room temperature conditions. As in the HHSTT scenario, applications occur at highly elevated temperatures. Therefore, it was important in Laird's research to understand the thermal environment and its impact to the development of gouging. Laird considered three sources of heat: aerodynamic heating, frictional heating, and chemical reaction.

Korkegi and Briggs observed very severe aerodynamic heating and friction at the HHSTT and developed a formulation for the slipper flowfield by considering a two dimensional model of the slipper as a blunt body moving parallel to a wall [4]. The researchers consider the gap between the slipper and rail to experience normal shock compression of the flow entering the gap. As the flow accelerates to sonic speeds boundary layers develop and merge to form a shear layer, which would lead to Couette flow. This Couette flow, as the researchers describe, is turbulent and compressible. They

conclude that the airflow is compressed to high pressures and temperatures and the aerodynamic heat rates are comparable to reentry vehicles as well as those of sliding friction for high bearing loads. This leads to the next source of heat which comes from friction.

An investigation of frictional heating by Krupovage and Rasmussen resulted in the power output developed by friction is directly proportional to the friction coefficient, pressure, and velocity [5]. This approach is similar to how the HHSTT researchers develop their analyses in that DADS utilizes the normal forces experienced on the rail and numerically solves equations of motion of a complex spring-damper system. The energy is assumed to be converted to heat and that half is dissipated into the slipper and half into the rail. The partition function that models the amount of heat generated between the slipper and rail is the subject of the present research and will be discussed in the subsequent chapters.

The final source of heat as defined by Laird is the oxidation of materials. At sufficiently high temperatures there are other effects that need to be considered in order to closely predict the thermal environment. One of which is the vibrational energy. For temperatures over 1000 K, this energy is increased at the molecular level and causes chemical reactions to occur in the sled components.

Further research by Meador in 2010 investigated the sliding contact wear at high velocities between the slipper and rail [8]. This is referred to as mechanical wear which involves the removal of material as a result of contact between two surfaces. Total wear is the combination of mechanical and melt wear, and the latter was evaluated in Meador's research by considering the heat conduction into the slipper due to friction. The fraction

of frictional heat energy going into the slipper was simplified by using a constant value as opposed to this current research which incorporates a partition function. In previous studies this value was set to 0.5 which constitutes a steady-state solution; however the HHSTT scenarios are very time dependent. Meador found it reasonable to use an average of 0.12 to 0.14 based on simulation runs for different values of the heat fraction.

In summary the previous research efforts discussed above have considered temperature effects in terms of friction, aerodynamics, and chemical reactions. This research focuses on the frictional energy produced between the slipper and rail interface and results in a temperature environment that eventually leads to melt wear.

## **II. Theory**

### **2.1 Chapter Overview**

This chapter will discuss the theory and motivation behind the research objective of determining how temperature affects the overall wear of sliding materials. When two materials slide against each other at a high velocity, the frictional energy produced is in the form of heat energy. There are three processes in which this heat is transferred between the two materials: conduction, convection, and radiation. This research involves the first two heat transfer methods. The final section of this chapter introduces an experiment by M. Wolfson conducted in 1960 [12]. It relates high speed travel under constant pressure and is used to compare current wear theory related to the HHSTT scenario.

## 2.2 Heat Transfer Equations

Moran et al. define heat transfer as the “energy in transit due to a temperature difference” [10]. When there exists a temperature gradient, heat transfer can occur. The first type is conduction. This type of heat transfer occurs when the slipper and rail are in contact with each other. It is reasonable to assume that the rail is stationary as the slipper slides down the track. The physical mechanism of conduction involves transferring energy from a high temperature to a low temperature. In this case, as the slipper slides down the rail, it is always moving into a colder region on the rail. Therefore, the heat transfer occurring between rail and slipper has the propensity to propagate into the rail. The equation for heat conduction is known as Fourier’s law and is expressed in Equation 2.1.

$$q_x'' = -k \frac{dT}{dx} \quad (2.1)$$

The heat flux  $q_x''$  is the heat transfer rate in the  $x$  direction per unit area perpendicular to the direction of flow, and it is proportional to the temperature gradient  $dT/dx$ . It has units of  $W/m^2$ . The proportionality constant  $k$  is a material property known as thermal conductivity, and the negative sign denotes the heat transfer in the direction of colder temperature.

The next heat transfer mode is convection. Moran et al. describe convection as the heat transfer between a surface and a moving fluid in which the two are at different temperatures [10]. This type of heat transfer occurs when the slipper and rail are not in

contact with each other. In some instances, the assumption of 100% contact may be made, but in the majority of this research, bouncing must be taken into consideration. Heat convection occurs from a stationary surface to a moving fluid. In this case, the surface is the rail and the moving fluid is the gap of air that exists between the rail and slipper. The temperature of the air is assumed to be ambient at the beginning, but as velocity increases, this temperature is greatly increased due to generated friction. The rate equation for heat convection is known as Newton's law of cooling and is expressed in Equation 2.2.

$$q_x'' = h(T_s - T_\infty) \quad (2.2)$$

The convective heat flux  $q_x''$  is proportional to  $h$  (W/m<sup>2</sup>·K) which is the material's convective coefficient and the temperature difference between the surface  $T_s$  and air  $T_\infty$ . There are two forms of convection: forced convection and free, or natural, convection. The difference lies in the nature of the flowing fluid. For the purposes of this research, the convection is considered free because the temperature variations in the air are assumed to be natural.

The third heat transfer mode is thermal radiation which involves emitting energy in the form of electromagnetic waves. The present research does not include thermal radiation but is a consideration for future research efforts.

### **2.3 Wolfson Experiment**

Over the past few years researchers at AFIT have been interested in a rocket test sled that was used in an experimental run at the HHSTT in January 2008. They were supplied with information characterizing the velocities and pressures of the slipper as it traveled down the track in the DADS data. The data set has been utilized in Matrix Laboratory (MATLAB) to characterize the total melt wear via a heat transfer and numerical analysis. The computational code to do this was first written by Hale in 2010 [2]. One of the objectives of this research was to compare the HHSTT experiment to M. Wolfson's experiment in 1960 [12]. In his work, high-speed wear was investigated with a test slipper made by the Stanford Research Institute (SRI). The following section discusses his research efforts and conclusions.

Wolfson's efforts were aimed at improving test track capability and increasing the wear resistance of the slipper. He noted that due to the excessive vibrational environment induced by the high velocity, slipper wear becomes a problem and can lead to catastrophic failure. In his research he teamed with the SRI and implemented a sophisticated test bed as the primary investigative tool. This model was capable of pneumatically loading a two-square-inch test sample at various pressures and velocities. This pneumatic is shown in Figure 2.5.

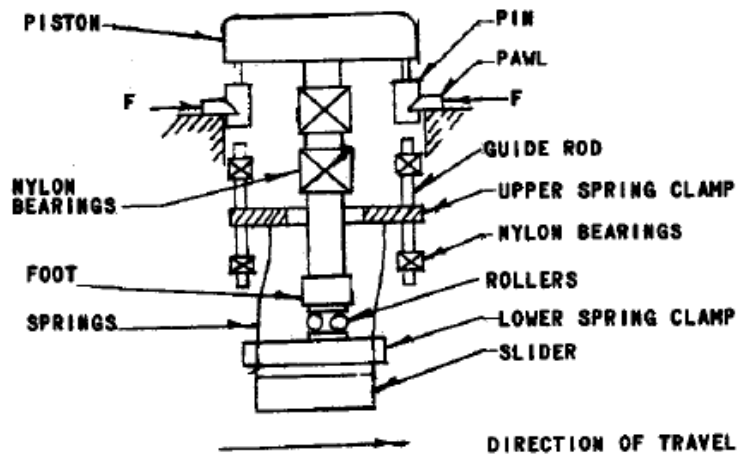


Figure 2.5: Frictional Energy Between Rail and Slipper [12]

The specific test plan that Wolfson implemented consisted of testing two velocities at three different pressures: 850 and 2,500 feet per second (ft/sec) over pressures of 300, 600, and 900 pounds per square inch (psi). The SRI bearing materials used were stainless steel 304 and molybdenum. At the conclusion of the test program Wolfson made the following postulates:

- The wear rate is time-dependent, increasing from a low initial value to a steady-state value.
- Melting of the bearing material is the primary mechanism for wear. This indicates that melting is a function of the material properties such as thermal conductivity and melting point. Molybdenum wore 10% more than stainless steel.

Wolfson also concluded that the wear rate on stainless steel increased with velocity and pressure, and these conclusions are in agreement with current wear theory. In his research he also discussed different coating techniques to reduce wear. At the time, technology limited these techniques to refractory metals and alloys; however he noted that the Holloman track had made an advance in reducing wear by utilizing track coatings. Wolfson noted the reasons for choosing metal coatings: to protect the rail from corrosion, to conduct heat to the rail, and to melt a thin surface layer and to absorb heat in doing so. In this current research, the discussion of coatings is not elaborated upon; however Wolfson made valuable conclusions in 1960 that has been beneficial to current wear theory.

Although Wolfson's experiment has been useful in developing the current wear theory, there are noted differences between the pneumatic test bed and the HHSTT test scenario. The HHSTT test scenario includes a phenomenon known as bounce where the slipper traverses down the track in a non-uniform manner. There are instances when the slipper is not in contact with the rail and bounces due to aerodynamic effects. Further, the HHSTT test does not deal with constant velocity and is highly time dependent. Nevertheless, the research that Wolfson performed in 1960 is a major accomplishment in understanding wear. The results of Wolfson and a comparison to the HHSTT scenarios are discussed in Chapter 4.

### III. Methodology

#### 3.1 Chapter Overview

This chapter covers the numerical development of the one-dimensional heat transfer analysis. The analysis begins by considering friction between the slipper and rail. This friction is translated into heat energy and the equations relating heat to the boundary conditions is based on Fourier's law of heat conduction. The melt phenomenon is introduced by considering the latent heat of fusion and is handled by a finite difference technique used in MATLAB. The final section of this chapter shows the MATLAB portion that incorporates the numerical analysis.

#### 3.2 Why Friction Matters

Friction is the force resisting relative motion of solid surfaces. In the HHSTT experiment, the two solid surfaces are the rail and slipper as depicted in Figure 3.6.

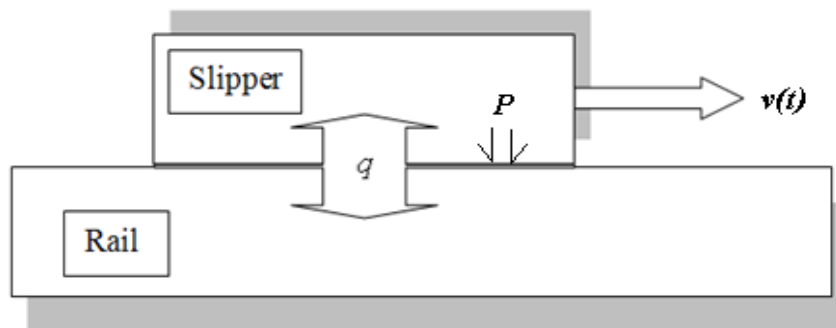


Figure 3.6: Frictional Energy Between Rail and Slipper

$P$  (Pa) is the loading pressure into the rail,  $v(t)$  (m/s) is the time dependent horizontal velocity of the slipper, and  $q$  (N·m/s) is the total frictional energy, or heat, that is

partitioned into the slipper and rail via the partitioning function. As the slipper slides against the rail, the frictional energy is continually passed into the bottom of the slipper. Eventually, when the frictional energy dominates the heating of the slipper, this leads to melting. The rate of energy  $q$  produced by frictional heat can be expressed as the product of the frictional force  $F_f(t)$  (N) and the sliding velocity as shown in Equation 3.6.

$$q(t) = F_f(t)v(t) \quad (3.3)$$

The frictional force is the product of the coefficient of friction  $\mu$  and the loading force into the rail. A friction coefficient versus the product of pressure and velocity was experimentally developed by Montgomery [9]. His studies focused on friction and wear at high speeds with particular interest in steel on steel materials. The Montgomery curve is shown in Figure 3.7. The asymptotic nature of this curve is an appropriate measure for the high velocities and pressures experienced in the HHSTT run; therefore, it has been utilized over the years for steel on steel sliding. The exponential curve fit is given in Equation 3.4.

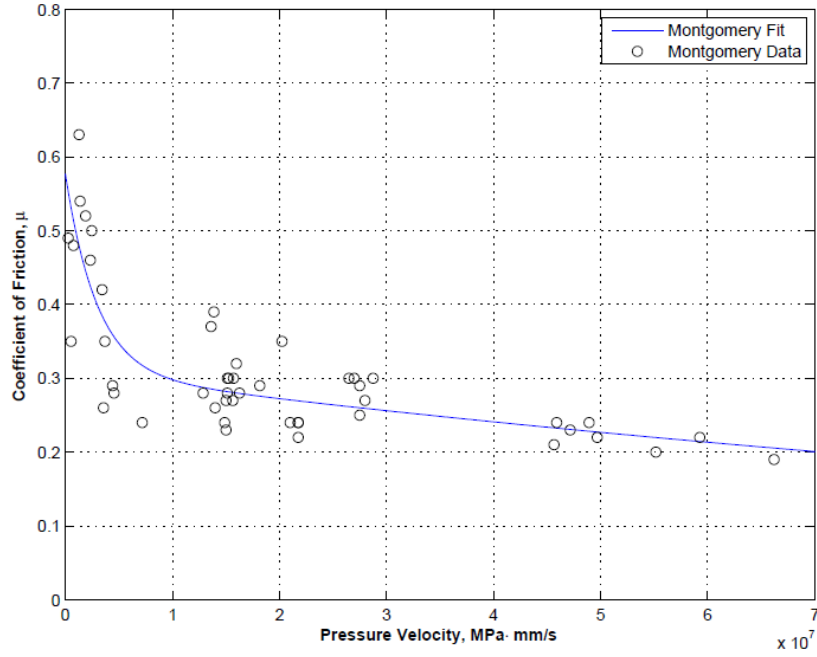
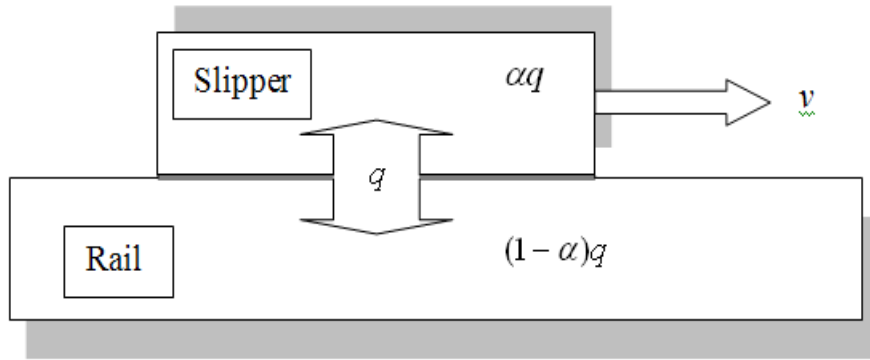


Figure 3.7: Montgomery Curve of Coefficient of Friction vs. Pressure Velocity[9]

$$\mu(Pv) = \begin{cases} 0.2696e^{-3.409 \times 10^{-7} Pv} + 0.3074e^{-6.08 \times 10^{-9} Pv} & : 0 < Pv < 4.45 \times 10^8 \\ 0.02 & : Pv \geq 4.45 \times 10^8 \end{cases} \quad (3.4)$$

The schematic in Figure 3.8 shows the relationship of the partition function  $\alpha$  which characterizes the fraction of heat flux entering into the slipper versus into the rail.



**Figure 3.8: Schematic showing Partition Function,  $\alpha$**

As the slipper travels along the stationary rail, the amount of heat energy  $q$  is partitioned into an amount of  $\alpha q$  into the slipper and  $(1-\alpha)q$  into the rail. At this point, the assumption is that the slipper is always in contact with the rail. There are a few characteristics of the partition function to note. The first is that it is a function of time. Second, that it evolves as the temperature difference between the slipper and the rail evolves. Paek-Spidell hypothesized this function based on experimental data of known melt wear [11]. The function is shown in Equation 3.5.

$$\alpha(t) = 0.4e^{-5t^2} + 0.1 \quad (3.5)$$

This proposed function assumes that at initial time, the heat energy is equally distributed between the slipper and the rail. As time increases and as the slipper's surface temperature rises, the partition function exponentially decays to an equilibrium value of 0.1. This value was chosen to match the assumption that by the end of the run the

fraction of heat generated into the slipper is 10%, where most of the energy is passed to the rail. The plot of  $\alpha$  versus time is shown in Figure 3.9.

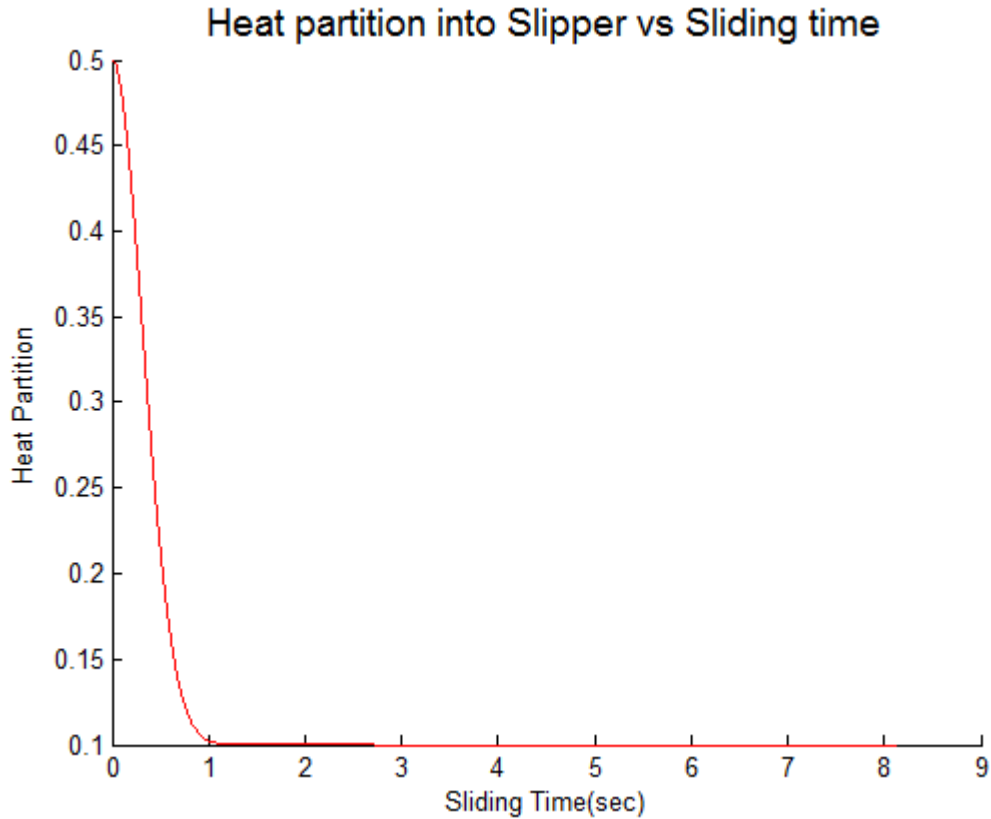


**Figure 3.9: Exponential Decay Partition Function vs. Time (Equation 3.5)**

From Figure 3.9 the function decays rapidly to 0.1 in approximately 1 second. Recall that this function assumes constant contact between the slipper and the rail. The next chapter will discuss other variations of the partition function that include the bounce condition and the tendency for the function to decay is less rapid. As stated previously,  $\alpha$  drives the amount of heat flux directed into the slipper. Mathematically, the equation for heat flux is expressed as Equation 3.6, where  $A_n$  is the contact surface area in  $\text{m}^2$ .

$$q(t) = \mu(t)F(t)v(t) \Rightarrow \begin{cases} q''_{slipper}(t) = \alpha(t) \frac{\mu(t)F(t)v(t)}{A} \\ q''_{rail}(t) = (1-\alpha) \frac{\mu(t)F(t)v(t)}{A} \end{cases} \quad (3.6)$$

### 3.3 Heat Flux Boundary Conditions

The one-dimensional heat conduction equation with constant thermal diffusivity  $\kappa$  is expressed in Equation 3.7.

$$\frac{\partial T}{\partial t} = \kappa \frac{\partial^2 T}{\partial x^2} \quad (3.7)$$

This equation is used to model the thermal evolution as time marches forward and as  $x$  is depth into the slipper. In the next section the partial derivatives are replaced with a difference quotient and the equation is numerically solved using the finite difference technique.

When the slipper slides along the rail, the major heat transfer mechanism is heat conduction. One of the boundary conditions is the frictional heat flux condition applied to the bottom surface of the slipper. This condition is called a Neumann boundary condition and is defined in Equation 3.8, where  $x$  is the distance into the slipper.

$$q'' = -k \left. \frac{\partial T}{\partial x} \right|_{x=0} \quad (3.8)$$

The above equation is based on Fourier's law of heat conduction when the slipper and

rail are in constant contact. Figure 3.10 depicts this condition where the assumption of flux is uniformly distributed along the contact surface.

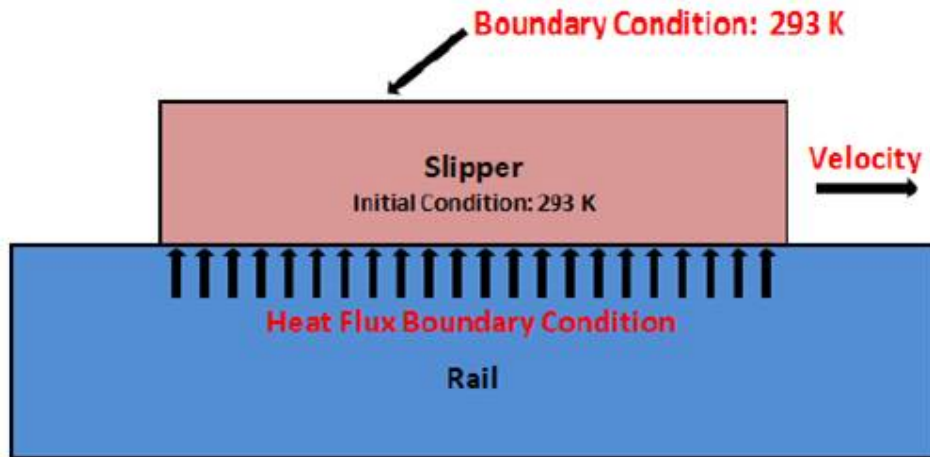


**Figure 3.10: Heat Transfer Boundary and Initial Conditions**

The upper boundary condition, called a Dirichlet condition, is at ambient temperature 293 K. The temperature profile of interest represents a small region at the surface of the slipper; therefore, an adiabatic assumption is plausible at the upper bound.

The DADS data contains the bounce condition which is characterized by the variation of the pressure distribution with time. If the pressure is less than some small number it is considered to be not in contact, and if it is greater than that small number, it is considered to be in contact. The DADS pressure data as shown in Figure 3.11, illustrates the large variation in pressure achieved as the slipper progresses along the rail. Notice the increased contact pressures which occur beginning about 3000 m down the rail.

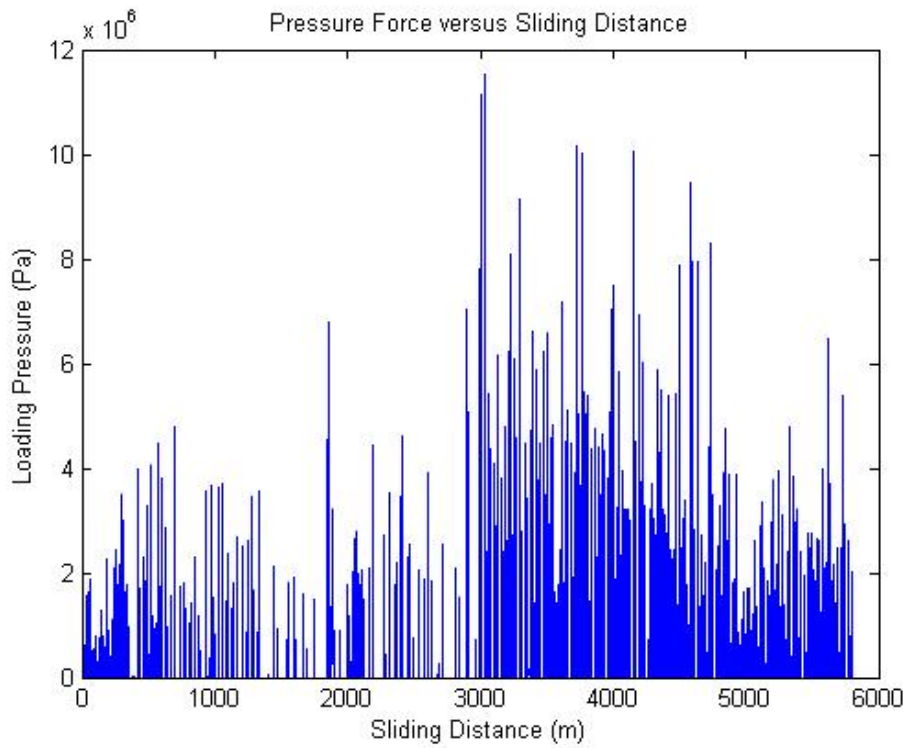


**Figure 3.11: DADS Pressure versus Sliding Distance**

This bouncing effect leads to a second heat transfer condition when the slipper and rail are not in contact with each other and that is the convective heat loss condition. The slipper's bounce impact is shown schematically in Figure 3.12.

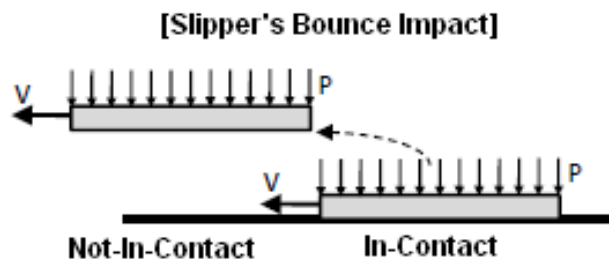


**Figure 3.12: Bouncing Effect**

The bouncing condition, a Robin boundary condition, is taken into effect in the MATLAB code via a switch function for in-contact and not-in-contact. The contact is determined from the DADS data. This switch function  $m$  is shown below in Equation 3.9.

$$m(t) = \text{sign}(\text{Force}) = \begin{cases} 1, & \text{Force is in contact} \\ 0, & \text{Force is not in contact} \end{cases} \quad (3.9)$$

The convective heat loss can be described with a second boundary condition in which a coefficient of convection  $h$  is introduced. For this research  $h$  is set to a constant value of  $100 \text{ W/m}^2\cdot\text{K}$ . It is also called the surface heat transfer coefficient. The convection heat equation is given in Equation 3.10.

$$q'' = h(T_s - T_\infty) \quad (3.10)$$

### 3.4 Heat Equation with Melt Consideration

In addition to the two heat transfer mechanisms described above, there is another phenomenon that occurs at the sliding surface of the slipper. This is described as melt when the frictional heat raises the temperature of the interface and reaches the melting temperature. When melt begins the depth of the melt layer increases and is removed immediately and continuously. Thus the surface temperature can never exceed the melting temperature, and therefore, the temperature at the onset of melt is equal to the

melt temperature. Prior to reaching the melt temperature, there exists the heat conduction boundary condition as described in Equation 3.8, and after reaching the melt time, it is necessary to introduce the heat loss due to latent heat of fusion,  $l$  (J/kg). The latent heat is the amount of energy required to convert a volume of solid material to a liquid at the same temperature. Figure 3.13 illustrates the evolution of temperature into the depth of the slipper as time progresses. At some time,  $t_m$ , the surface temperature reaches the melt temperature. After the time of melt ( $t_m$ ) the surface exceeds the melt temperature and a melt layer begins to develop. This melt layer has a thickness of  $\sigma$  and is illustrated by the shaded depth.

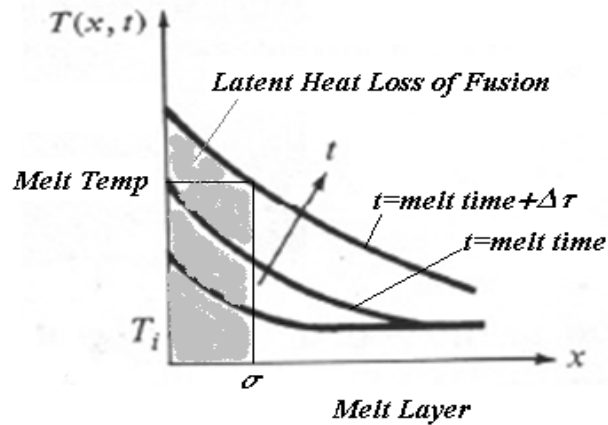


**Figure 3.13: Melt Layer**

From Figure 3.13, the first line represents the temperature profile into the depth of the slipper at some time before melt time. The next line represents the temperature profile at the onset of melt, and finally at the next time increment  $\Delta t$  the temperature exceeds melt by a distance  $\sigma$ . Therefore the melt layer  $\sigma$  has exceeded the melt temperature via the conductive heat loss from Equation 3.7, and in order to correct the analysis the latent heat

of fusion must be included. The boundary condition is modified as shown in Equation 3.11.

$$-k \frac{\partial T_f}{\partial x} \Big|_{x=\sigma(t)} = m(t) \underbrace{\left( \alpha \frac{q(t)}{A} - \rho l \frac{d\sigma}{dt} \right)}_{\text{Heat Conduction}} + [1 - m(t)] \underbrace{h(T_f - T_i)}_{\text{Heat Convection}} \quad (3.11)$$

Another way to write this equation is piecewise as shown in Equation 3.12. This equation says that the heat flux condition with  $\sigma(t)$ , the location of the melt front, is equal to moving a distance  $d\sigma$  in the  $x$  direction during a time  $dt$ , for the in-contact region. While not in contact, the condition remains as the convective heat loss.

$$-k \frac{\partial T_f}{\partial x} \Big|_{x=\sigma(t)} = \begin{cases} \alpha \frac{q(t)}{A} - \rho l \frac{d\sigma}{dt} & \text{in contact} \\ h(T_s - T_\infty) & \text{not in contact} \end{cases} \quad (3.12)$$

### 3.5 How the Melt Layer is Developed Numerically

The melt front has been established as  $\sigma(t)$  where  $t > 0$ . If the melt layer is removed, the temperature at the boundary cannot exceed the material's melt temperature,  $T_m$ . Therefore, the temperature at  $\sigma(t)$  is  $T_m$ . Heat flow into the slipper must also be determined at some distance  $x$  into the slipper. This boundary condition far from the contact surface is taken to be the fixed ambient temperature,  $T_a$ . The aforementioned boundary conditions are summarized in Equation 3.13 and 3.14.

$$T(\sigma(t), t) = T_m \quad (3.13)$$

$$T(x, t) = T_a \quad (3.14)$$

$T_a$  is far enough away to from the contact boundary to consider it as the temperature at the top surface of the slipper. However, for computational reasons, the boundary condition in Equation 3.14 can be replaced with Equation 3.15.

$$T(x^* + \sigma(t), t) = T_a \quad (3.15)$$

$x^*$  is a sufficiently large distance. For this application the diffusion length is chosen. It is given in Equation 3.15 where  $t^*$  is time of event which is approximately 6 seconds for the HHSTT scenario.

$$x^* = \sqrt{\frac{k}{\rho c} t^*} \quad (3.16)$$

This sets the bounds on the slipper computational region. The initial conditions on the slipper are described below in Equations 3.17 and 3.18, which state that there is no melt front initially, and the initial temperature is at some prescribed ambient temperature,  $T_a$ .

$$\sigma(0) = 0 \quad (3.17)$$

$$T(x, 0) = (T_m - T_a)\varphi(x) + T_a \quad (3.18)$$

Further it is convenient to introduce a non-dimensional function  $\varphi(x)$  such that the property  $\varphi(0) = 1$  and as  $x \rightarrow \infty$   $\varphi(x) \rightarrow 0$ . However, the melt creates a new problem, and the conditions change at this point. Up to now the initial condition was  $T_a$  at time  $t = 0$ . When melt occurs, the condition is changed to represent a new time, the melt time  $t_m$  and at  $t = t_m$  the temperature is  $T_m$ .

### 3.5.1 Finite Difference Method

In the previous section the one-dimensional heat equation is expressed as a parabolic partial differential equation in Equation 3.8. In this section the equation is replaced with a finite difference scheme using a forward difference pattern on the left hand side and a central difference pattern on the right hand side as shown in Equation 3.19.

$$\frac{T_i^{n+1} - T_i^n}{\Delta t} = \kappa \frac{T_{i+1}^n - 2T_i^n + T_{i-1}^n}{(\Delta x)^2} \quad (3.19)$$

Figure 3.14 represents a schematic for the slipper surface and node spacing for the finite difference equation where  $i$  is the running index in the  $x$  direction and  $n$  is the running index in the  $t$  direction, where  $x$  and  $t$  are distance and time, respectively.

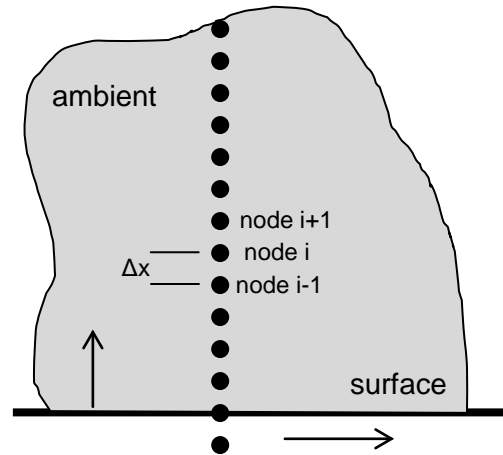


**Figure 3.14: Slipper Surface and Node Spacing**

Rearranging Equation 3.19 provides a solution for temperature in the time marching index.

$$T_i^{n+1} = T_i^n + \kappa \frac{\Delta t}{(\Delta x)^2} (T_{i+1}^n - 2T_i^n + T_{i-1}^n) \quad (3.20)$$

Now consider an explicit finite difference module shown in Figure 3.15. Note that the time axis is in the vertical direction, and the  $x$  direction is along the abscissa.

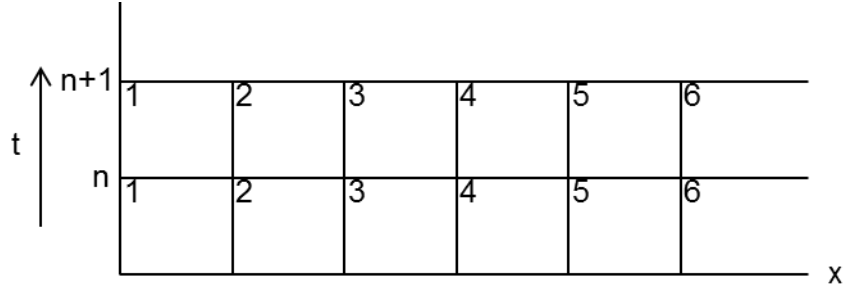


**Figure 3.15: Explicit Finite Difference Module**

At  $n = 1$  the node represents the flux condition yielding the temperature  $T$  at  $T_1$ . This is incrementally built upon for  $\Delta t$ . Therefore, at time  $n+1$  considering the module above, the equations would yield the following as shown below in Equations 3.21 and 3.22.

$$T_2^{n+1} = T_2^n + \kappa \frac{\Delta t}{(\Delta x)^2} (T_3^n - 2T_2^n + T_1^n) \quad (3.21)$$

$$T_3^{n+1} = T_3^n + \kappa \frac{\Delta t}{(\Delta x)^2} (T_4^n - 2T_3^n + T_2^n) \quad (3.22)$$

Note that this is done for all the grid points including the boundary conditions. For example, grid point 1 in Figure 3.15 is the initial condition due to the frictional heat flux. Grid point 6 is the upper boundary which for this analysis is assumed to be infinity with the ambient temperature equal to 293 K.

However, once melt is introduced, the problem becomes more complex. As the heat (temperature) flow is developed into the slipper, there is some specific time when the boundary between the slipper and the rail reaches the melt temperature  $T_m$ . The next

time increment  $\Delta t$  produces a temperature distribution without considering the latent heat of fusion. This temperature distribution will have a surface temperature that exceeds  $T_m$ . Because the surface temperature exceeds melt and melt removal is being considered, the analysis must be corrected by using the heat flux condition in Equation 3.12. The melt front is located at some distance  $\Delta\sigma$  at the time increment  $\Delta t$ . This is found by taking the temperature at the slipper surface and determining if the first node inside the slipper which has not reached melt and obtaining its temperature as seen in Figure 3.13. The melt front is then determined by interpolating between temperatures exceeding  $T_m$  and below  $T_m$ . Thus it is a straight line calculation shown in Equation 3.23.

$$T_{@surface} - T_{@node\ inside\ mesh} = \Delta\sigma \quad (3.23)$$

The analysis continues by again solving for the heat flux  $q_x''$  in Equation 3.24 and finding a new thermal distribution.

$$q_x'' = \frac{\alpha\mu F_v}{A} - \rho l \frac{d\sigma}{dt} \quad (3.24)$$

When melt is identified as  $\Delta\sigma$  at the first time increment  $\Delta t$ ,  $d\sigma/dt$  can be replaced with  $\Delta\sigma/\Delta t$ ; therefore, Equation 3.24 may be written as the following.

$$q_x'' = \frac{\alpha \mu F v}{A} - \rho l \frac{\Delta \sigma}{\Delta t} \quad (3.25)$$

In order to prevent the numerical position of the nodes from shifting for every new  $\Delta \sigma$ , it is added to the upper end so that the distance  $L$  in Figure 3.16 is always the same. This assumes the upper bound to the ambient temperature  $T_a$  is far enough away to say that the boundary does not affect the temperature flow.

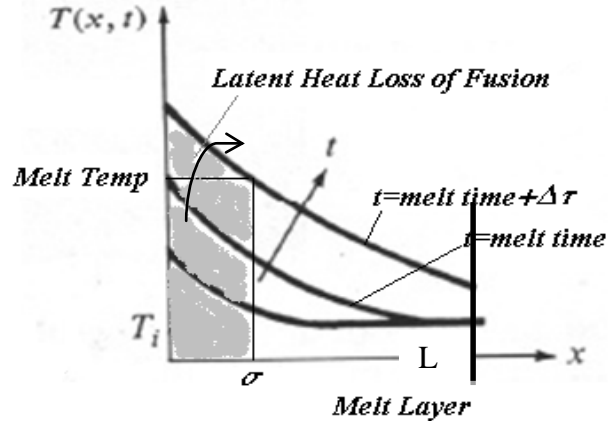
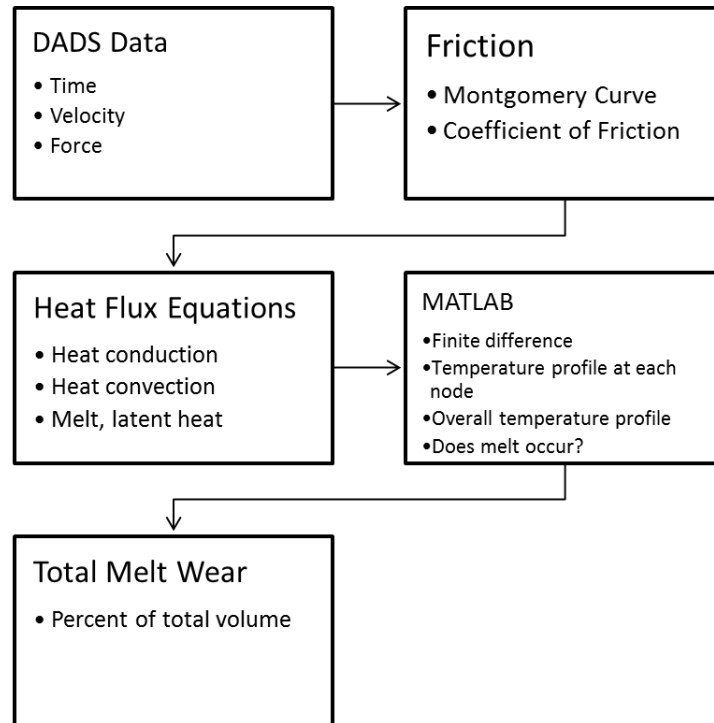


Figure 3.16: Melt Layer

The next section discusses the computation code utilized in MATLAB that incorporates the heat flux equations and the numerical finite difference scheme to solve for the temperature distribution through the slipper. The outcome is a prediction of total melt wear. Figure 3.17 is a flow chart describing how the analysis is performed using the DADS data, heat flux equations, and numerical solution produced in MATLAB to predict the total melt wear.



**Figure 3.17: Analysis Flow Chart**

### 3.6 Understanding the MATLAB Code

The heat transfer analysis takes place in a MATLAB script that computationally solves for total melt wear percentage. This section describes the each portion of the code and how it is used in the analysis.

There are two MATLAB scripts used in this analysis. The first one loads DADS data and creates a database of all the variables of interest: time, velocity, and force. The following is an excerpt of the file.

```

% load the data file
load DADS_Jan2008_alldata_refined

% DADS analysis time array
time = DADS_Jan2008_noheader_alldata_refined(:,1);

% sled center of gravity velocity data
vsled_horiz = DADS_Jan2008_noheader_alldata_refined(:,7);
vsled_lat = DADS_Jan2008_noheader_alldata_refined(:,5);
vsled_vert = DADS_Jan2008_noheader_alldata_refined(:,6);

```

```

% front right slipper contact forces
f_fr1 = DADS_Jan2008_noheader_alldata_refined(:,34);
f_fr3 = DADS_Jan2008_noheader_alldata_refined(:,36);
f_fr4 = DADS_Jan2008_noheader_alldata_refined(:,37);
f_fr6 = DADS_Jan2008_noheader_alldata_refined(:,38);

```

The main code takes the saved variables from this file and performs the heat transfer analysis. The first section defines the time and velocity variables and sets the material constants. The material constants include specific heat, thermal conductivity, thermal diffusivity, and the geometry of the slipper.

```

% Load Data
dataDADS = load('DADS_Jan2008_alldata_refined');

time = DADS_Jan2008_noheader_alldata_refined(:,1);
cg_horiz = DADS_Jan2008_noheader_alldata_refined(:,4)*.0254;
vsled_horiz = DADS_Jan2008_noheader_alldata_refined(:,7)*.0254;
% Set Material Constants
Cp_air = 1004; % specific heat, J/(kg K) for 298K
Cp_He = 5193; % specific heat, J/(kg K) for 298K
Tinit = 293; % initial temperature, K

% Set Slipper Constants
Sw = 4*0.0254; % slipper width, m
Sl = 8*0.0254; % slipper length, m
An = Sw*Sl; % slipper area, m^2 ( = 32 sq in)
thickness = 14.7E-3; % slipper thickness, m (14.7 mm)
vol = An * thickness; % slipper "plate" volume, m^3
rho_V300 = 8000; % density, kg/m^3
mass = rho_V300 * vol; % single slipper mass, kg
Cp_V300 = 420; % specific heat, J/(kg K)...at 700K
numslippers = 4; % number of slippers in the sled
Tmelt = 1685; % V300 melt temperature
Km = 31; % thermal conductivity of slipper, J/(m s K)
Kr = 15; % thermal conductivity of rail
alpha = Km/(rho_V300 * Cp_V300); % thermal diffusivity of metal, m^2/s
H_VM300 = 2e9; % Slipper Hardness (Pa)

```

The next part of the code defines the partition function. This function uses the time array variable that was previously defined and creates an array that contains a partition value for each increment of time. The formulation is based on the mathematics

of a Gaussian distribution and is arbitrary in nature. Therefore, as part of the analysis, other assumed formulas for the partition function are introduced in Chapter 4.

```
% (1) Exponential Function
SlipPartition = exp((-time.^2)*5)*.4+.1;
```

The next section of the code introduces friction by utilizing the DADS pressure velocity data and the Montgomery curve to determine the coefficient of friction (COF). Pressure is determined by calculating force over surface area. The coefficient of friction is based on the Montgomery curve in Figure 3.7. For a given value of pressure velocity, the COF is determined by either Montgomery's equation or a constant value of 0.02.

```
force_data= (DADS_Jan2008_noheader_alldata_refined(:,46) +
DADS_Jan2008_noheader_alldata_refined(:,47))*4.448;
% contact force between bottom of slipper/top of rail (Newtons)

P = force_data/(An*slideCont);           % pressure (Pa N/m^2)
PV = (P*10^-6).*(vsled_horiz*1000);      % used to find Montgomery's COF

COF = zeros(length(PV),1);

for index = 1:length(COF)
    if PV(index) < 4.45e8
        COF(index) = 0.2696*exp(-3.409e-7*PV(index))+0.3074*exp(-6.08e-
9*PV(index));                            % Montgomery's equation
    else
        COF(index) = 0.02;
    end
end
```

Once the friction coefficient is determined it is used in the heat flux equation as described in the previous section.

```
HeatFlux=SlipPartition.*P.*vsled_horiz.*COF;           % (Watts/m^2)
```

The finite difference method is used to determine the temperature profile of the slipper. As discussed in the previous section, a boundary condition is chosen such that heat conduction occurs at the surface of the slipper where only the direction into the

slipper is considered. The heat conduction equation is replaced with a finite difference grid of 100 points as shown in the code below. In the grid the  $x$  direction represents space marching and  $t$  represents time marching.

```
% Calculate Temperature Profiles Using Finite Difference Method
% spatial discretization
M = 100; %number of spatial steps
dxi = 1/M;
xi = (0:dxi:1);
% temporal discretization
N = length(time); %number of time steps
dt = time(2)- time(1);
```

The next section of the code introduces the bounce condition where the sign of the force data, whether positive or negative, determines whether the slipper is or is not in contact with the rail. If the sign is positive, the slipper is in contact. If the sign is negative, the slipper is not in contact.

```
% On/Off switch for boundary condition
m = sign(force_data);
```

Another parameter defined in the code is  $x^*$  where this is a sufficiently large distance away from the boundary and represents the upper bound.

```
xstar = sqrt(alpha*time(end));
```

The next section sets the initial conditions where  $\sigma$  is the location of the melt front and  $d\sigma/dt$ , or sigma dot, is the melt rate. Both are initially zero.

```
%value initialization
sigma = zeros(1,N);
sigmadot = zeros(1,N);
```

The MATLAB code for the finite difference scheme is found in Appendix B. It takes the grid points and solves for the temperature profile at each point and continues until the temperature distribution reaches melt. When the boundary condition exceeds

the melt temperature, a new condition is considered that involves the latent heat of fusion. This is a numerical method of solving for the temperature profile and provides the solution for total melt wear of the slipper. The melt wear percentage is the percent of thickness worn with respect to the entire thickness. “Sigma” in the code is the accumulated wear depth at each time step.

```
melt_wear=(sigma/thickness*100);  
TotalMeltWear=melt_wear(end)
```

## **IV. Analysis and Results**

### **4.1 Wolfson Experiment Results**

This section describes several scenarios relating to the Wolfson experiment. Wolfson’s experiment in 1960 consisted of applying constant bearing pressure at constant velocity. The scenarios discussed here were initially considered in order to evaluate and exercise the MATLAB code previously discussed. Each part of the analysis was evaluated and modified as necessary before being used in the Holloman scenario. The Wolfson experiment used an apparatus that consisted of a two inch by two inch square piece and pneumatically applied on a track at constant pressure. Reference Figure 2.5 in Chapter 2. It traveled a distance of 609.6 m (2000 ft) at constant velocity. There were three pressures and two velocities as well as two materials tested. The three pressures were 2.07, 4.14, and 6.21 MPa (300, 600, and 900 psi). The velocities were 251 and 762 m/s (850 and 2500 ft/s), and the two materials tested were stainless steel 304 (SS) and molybdenum (Mo). Table 1 below describes the 12 different scenarios that were exercised in the code.

**Table 1: Wolfson Scenarios**

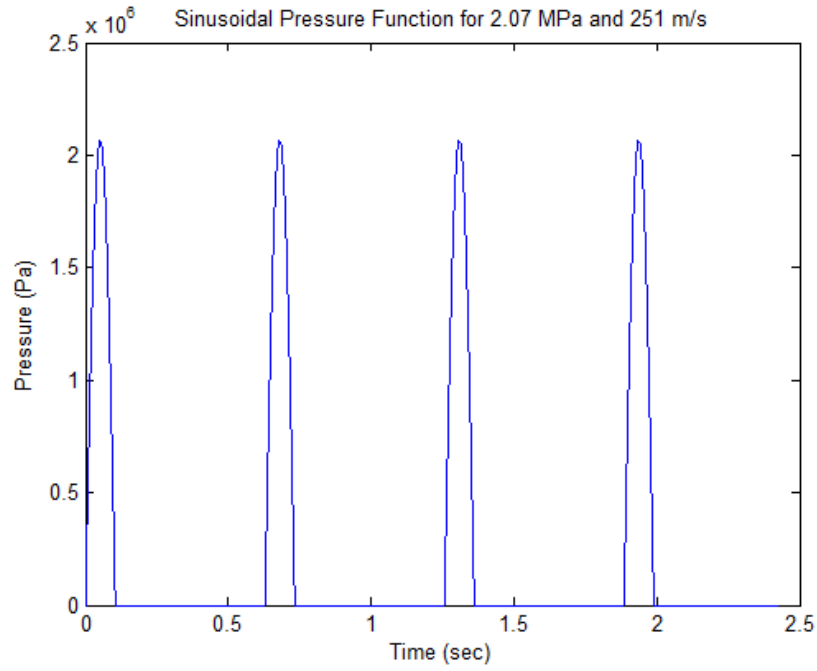
<b>Material 1: Stainless Steel 304</b>	<b>Material 2: Molybdenum</b>
Pressure 1: 2.07 MPa Velocity 1: 251 m/s	Pressure 1: 2.07 MPa Velocity 1: 251 m/s
Pressure 1: 2.07 MPa Velocity 2: 762 m/s	Pressure 1: 2.07 MPa Velocity 2: 762 m/s
Pressure 2: 4.14 MPa Velocity 1: 251 m/s	Pressure 2: 4.14 MPa Velocity 1: 251 m/s
Pressure 2: 4.14 MPa Velocity 2: 762 m/s	Pressure 2: 4.14 MPa Velocity 2: 762 m/s
Pressure 3: 6.21 MPa Velocity 1: 251 m/s	Pressure 3: 6.21 MPa Velocity 1: 251 m/s
Pressure 3: 6.21 MPa Velocity 2: 762 m/s	Pressure 3: 6.21 MPa Velocity 2: 762 m/s

Each scenario underwent the same analysis utilized in the HHSTT MATLAB code. First, the material properties were changed to match either SS or Mo, and second, the velocity, pressure and travel distance were each set to a constant. In order to closely match the HHSTT experiment which involved the bounce condition that was estimated at 30% contact time between the rail and slipper, the pressure was defined as a half sinusoidal wave function. The positive values represented in-contact, and the negative values were set to zero and represented not-in-contact. The amount of travel time for each run was based on the given velocity and constant distance of 609.6 m. For the low velocity case, 251 m/s, the run time was 2.4 seconds, and for the high velocity, 762 ft/s, the run time was 0.8 seconds. Therefore, there was less contact time for the high velocity scenarios. Equation 4.26 is the nominal pressure function where  $P_0$  is the constant pressure and  $\omega$  is a chosen frequency.

$$P = P_0 \sin(\omega t) \tag{4.26}$$

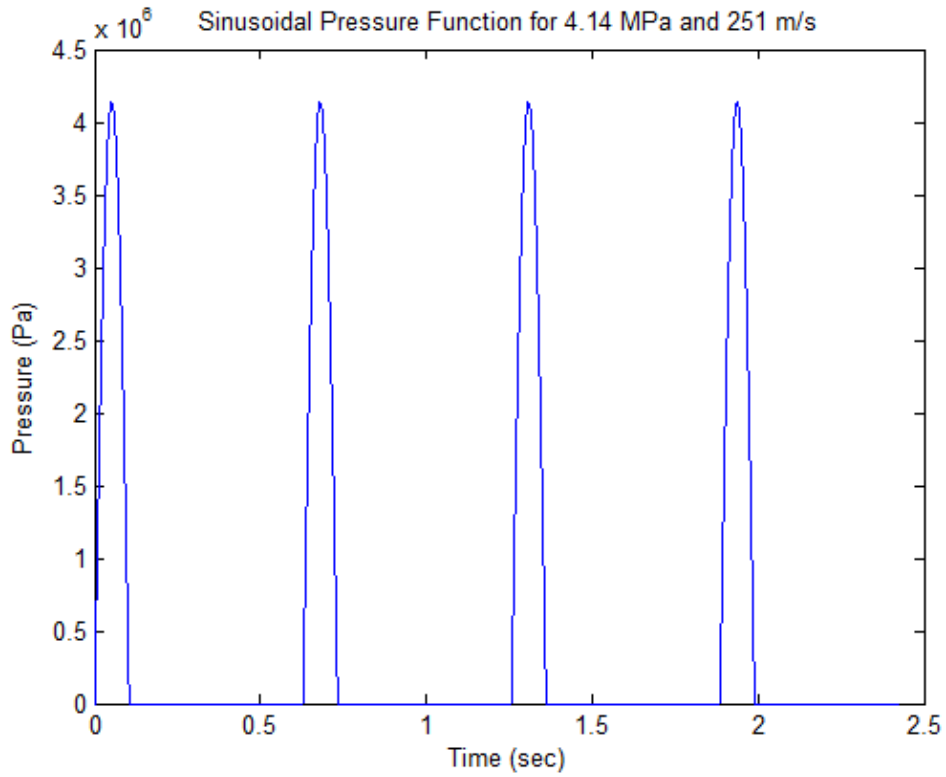
Although Wolfson reported that the pneumatic applied a constant bearing pressure, it was estimated that bounce was present given the technology in 1960 and similarity to the HHSTT test. Therefore, the frequency chosen was 30 Hz which equates to a cycle every 0.03 seconds. By assuming this frequency, the pressure function represents in contact for the positive values and not in contact for values set to zero. Furthermore, it was assumed that the constant bearing pressures that Wolfson reported were not attainable for the run duration; therefore, the amplitude of the sine wave was chosen to represent the peak

pressure. The following Figures 4.18 to 4.23 represent the pressure versus time function given in Equation 4.26.



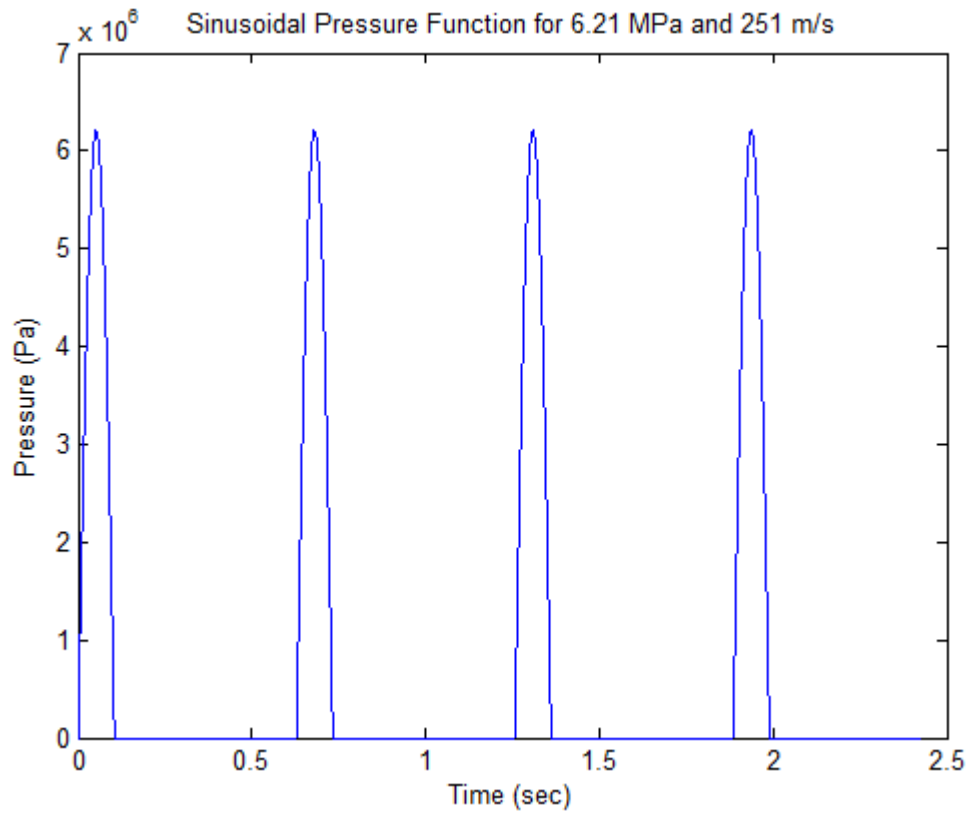
**Figure 4.18: Pressure Function for 2.07 MPa, 251 m/s**

Figure 4.18 represents the half sine wave function at an amplitude of 2.07 MPa. The velocity is 251 m/s. The peaks indicate the in-contact periods for this scenario and the zero values represent no contact.



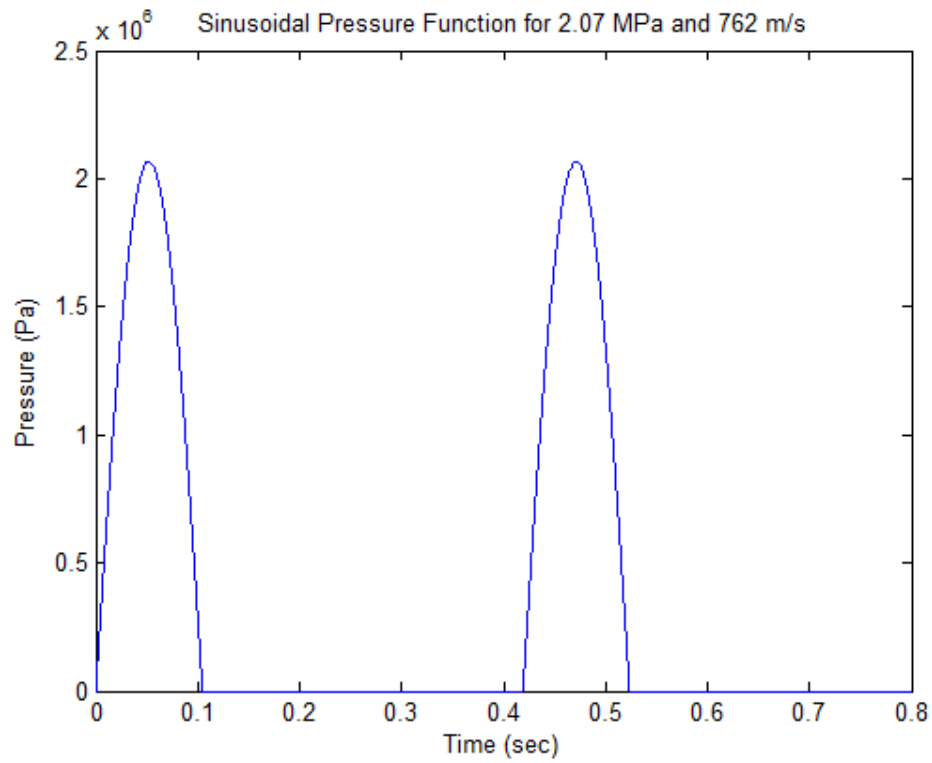
**Figure 4.19: Pressure Function for 4.14 MPa, 251 m/s**

Figure 4.19 represents the half sine wave function at an amplitude of 4.14 MPa, equivalent to 600 psi. The period for this function is identical to the previous figure given the same constant velocity of 251 m/s.



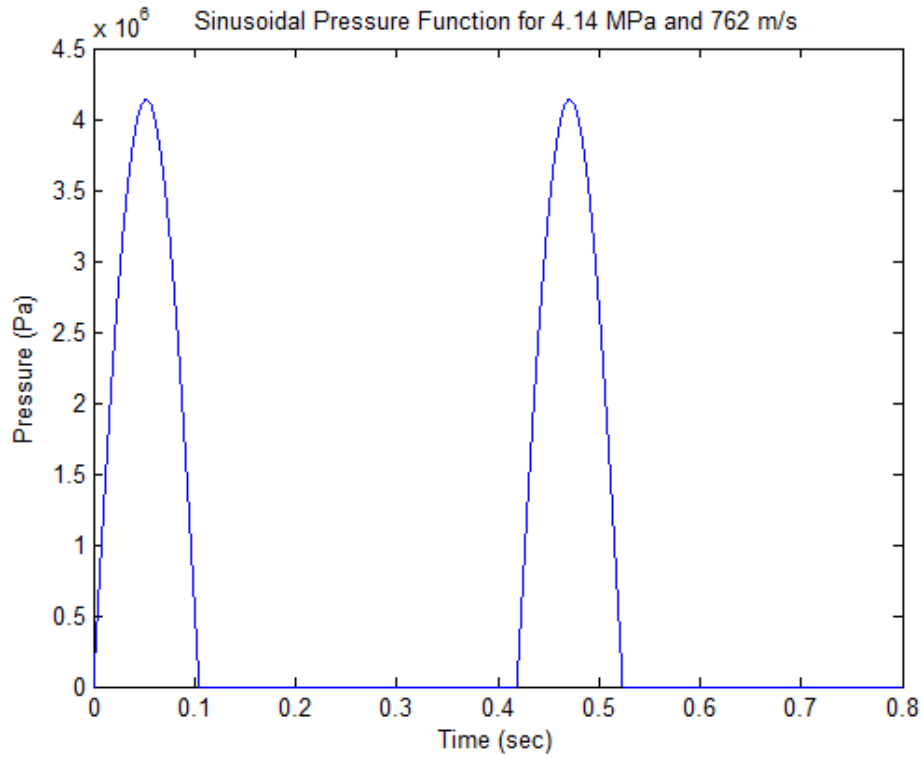
**Figure 4.20: Pressure Function for 6.21 MPa, 251 m/s**

Figure 4.20 represents the half sine wave function at an amplitude of 6.21 MPa, equivalent to 900 psi. The period for this function is identical to the previous figures given the same constant velocity of 251 m/s. The next three figures show the pressure functions for the scenarios involving the velocity at 762 m/s.



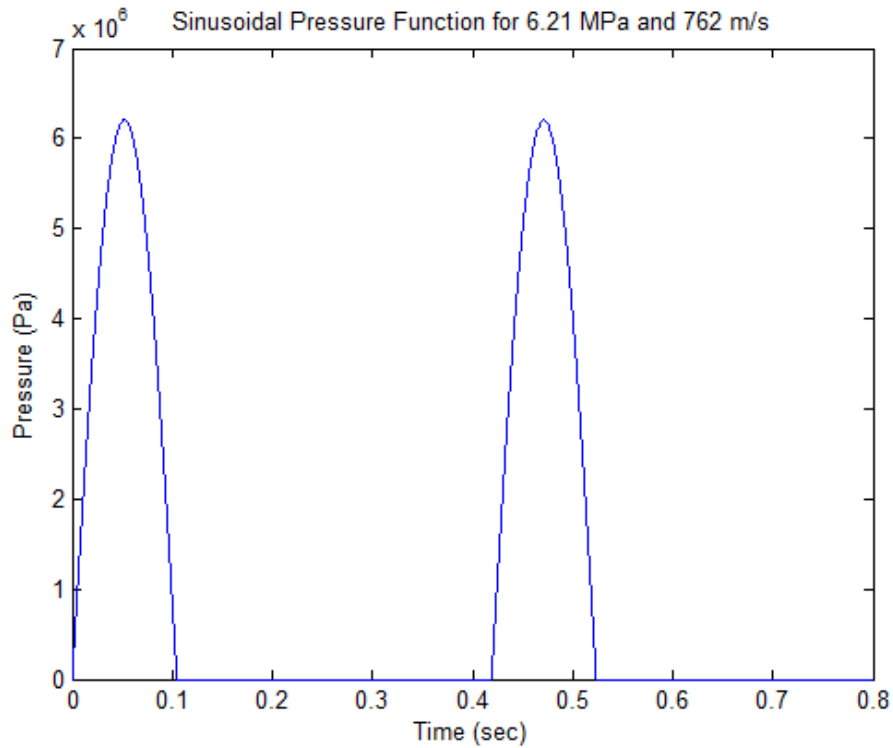
**Figure 4.21: Pressure Function for 2.07 MPa, 762 m/s**

Figure 4.21 represents the half sine wave function at an amplitude of 2.07 MPa, equivalent to 300 psi. Note that the period has changed because the velocity is now 762 m/s. The total run time for this scenario is 0.8 seconds.



**Figure 4.22: Pressure Function for 4.14 psi, 762 m/s**

Figure 4.22 represents the half sine wave function at an amplitude of 4.14 MPa, equivalent to 600 psi. The period and total run time is identical to the previous figure.



**Figure 4.23: Pressure Function for 6.21 MPa, 762 m/s**

Figure 4.23 represents the half sine wave function at an amplitude of 6.21 MPa, equivalent to 900 psi. This is the final pressure profile for the Wolfson scenarios.

The partition function used for each scenario was the exponential decay function that was described in Chapter 3 in Equation 3.5. This function, which was hypothesized, says that 50% of the heat is transferred into the rail initially and exponentially decays to a steady state value. As the slipper travels along the rail, it is always moving into a colder region, while the slipper continues to heat up. Each Wolfson scenario was applied in the MATLAB code and evaluated for surface temperature and if melt occurred. The following figures show the results for each velocity and pressure, low to high, with stainless steel 304 results first followed by molybdenum.

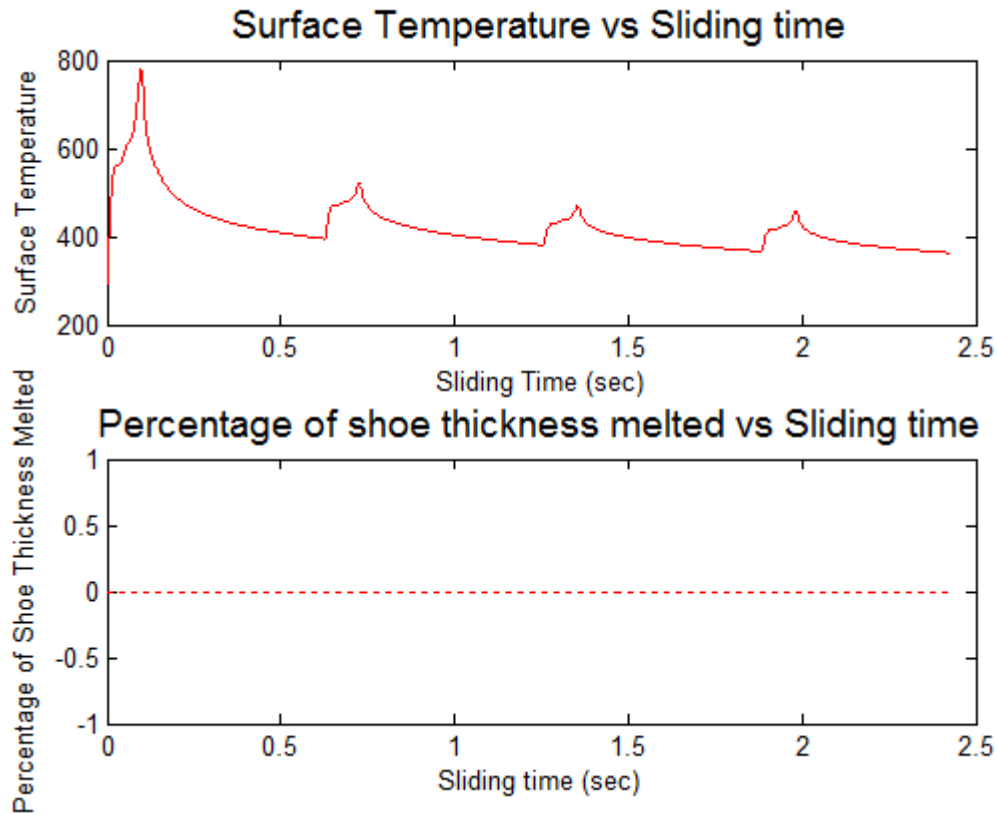


**Figure 4.24: SS: Pressure 2.07 MPa, Velocity 251 m/s, Surface Temperature and % Melt vs. Time**

Figure 4.24 in the top plot shows the surface temperature versus sliding time for stainless steel 304 with a bearing pressure of 2.07 MPa and constant velocity of 251 m/s. The peaks in the temperature plot represent when the pneumatic piece is in contact and correlate with the pressure profile shown in Figure 4.18. While in contact the material heats up, and when not in contact, the temperature decreases and experiences cooling. At the next instance of contact the temperature begins to rise again but does not reach the previous maximum temperature. This is due to the partition function as it decays over time. The spikes observed in the latter three peaks are a feature of numerical calculation in MATLAB. This behavior is observed in the figure above and

the subsequent figures show similar characteristics. The melting temperature of this metal is 1610 K and the maximum surface temperature reached was 784 K. As a result, no melt occurred as shown.

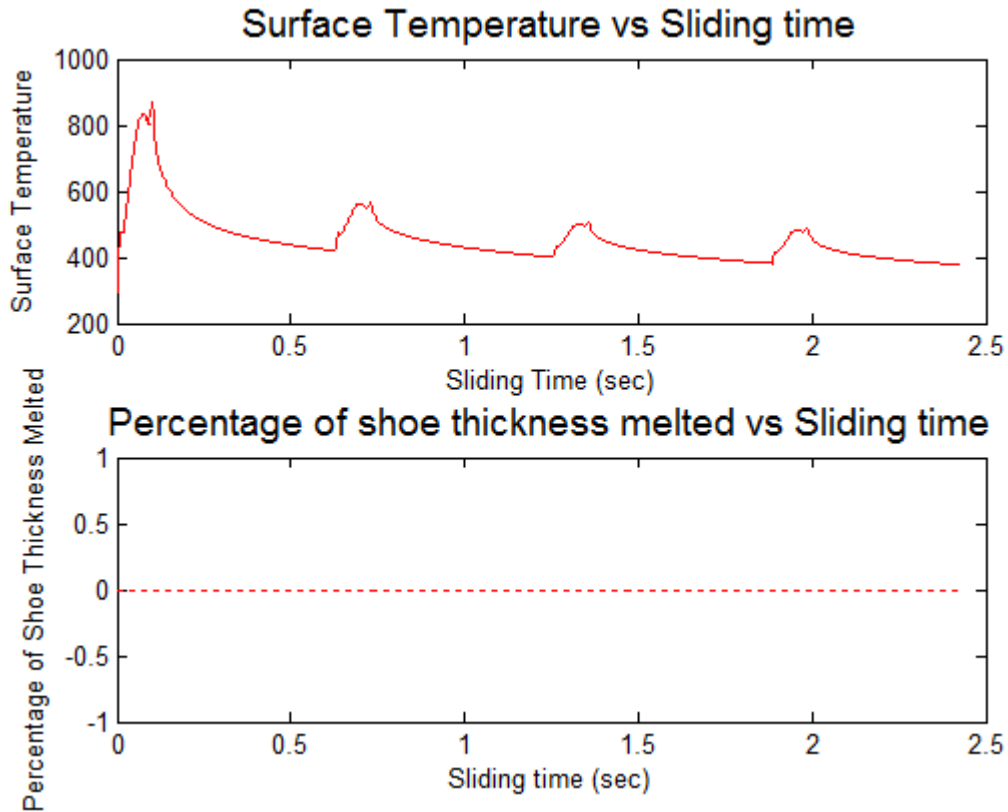


**Figure 4.25: SS: Pressure 4.14 MPa, Velocity 251 m/s, Surface Temperature and % Melt vs. Time**

Figure 4.25 in the top plot shows the surface temperature versus sliding time for stainless steel 304 with a bearing pressure of 4.14 MPa and constant velocity of 251 m/s. The temperature profile corresponds with the sinusoidal pressure profile shown in Figure 4.19. At each point in contact the temperature begins to rise due to the frictional heat energy being generated. When it is not in contact the temperature decreases, and at the next point in contact the temperature increases. This pattern is repeated for the duration

of time. The maximum surface temperature reached was 870 K but was below the melting temperature. As a result, no melt occurred.

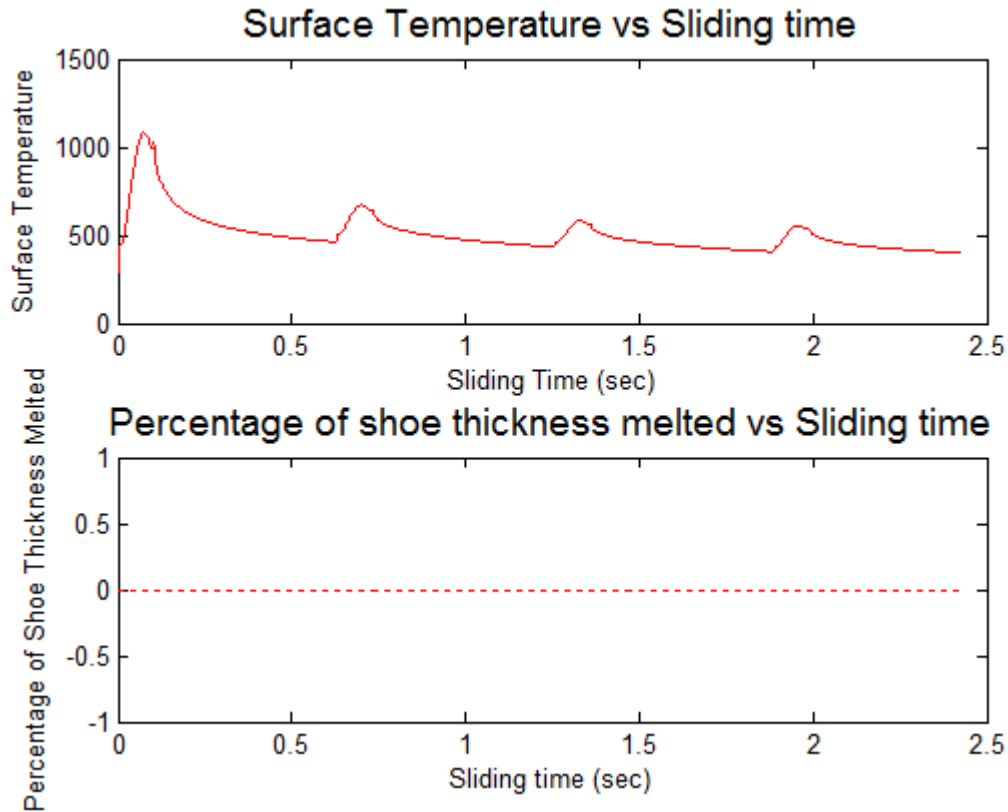


Figure 4.26: SS: Pressure 6.21 MPa, Velocity 251 m/s, Surface Temperature and % Melt vs. Time

Figure 4.26 in the top plot shows the surface temperature versus sliding time for stainless steel 304 with the highest bearing pressure of 6.21 MPa and constant velocity of 251 ft/s. The temperature profile corresponds with the sinusoidal pressure profile shown in Figure 4.20. At each point in contact the temperature begins to rise due to the frictional heat energy being generated. When it is not in contact the temperature decreases, and at the next point in contact the temperature increases. This pattern is

repeated for the duration of time. The maximum surface temperature reached was the highest at 1082 K but was still below the melting temperature. As a result, no melt occurred. The next few figures show the same data but with the higher velocity at 762 m/s.

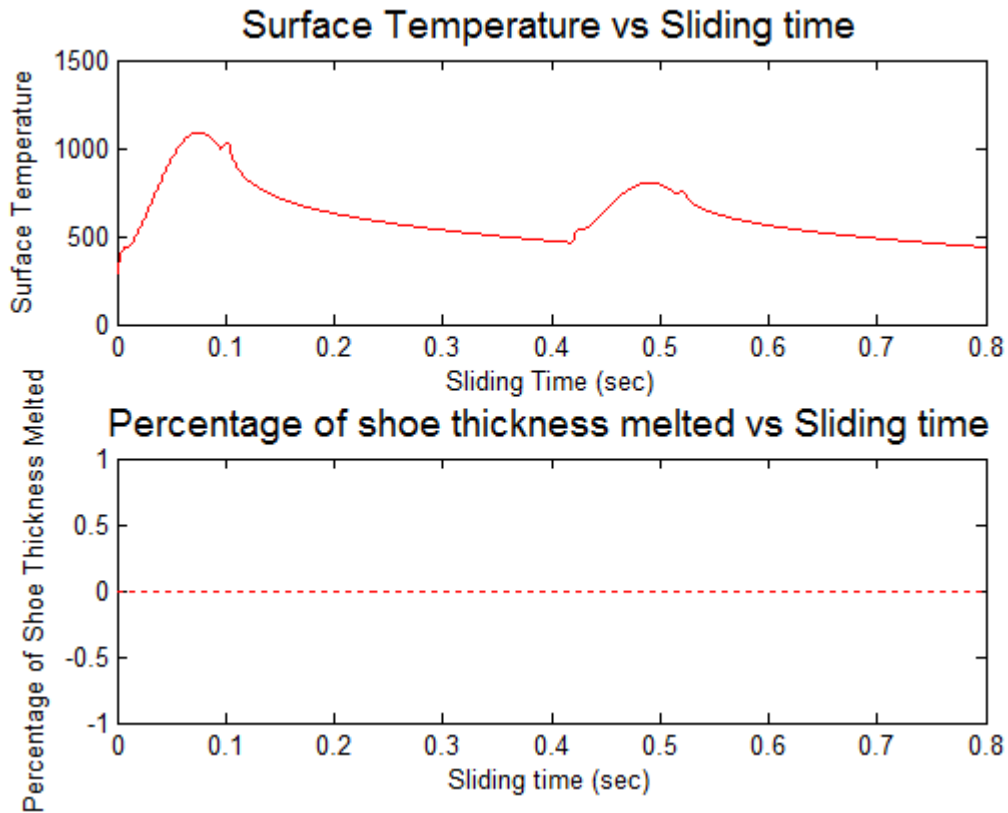
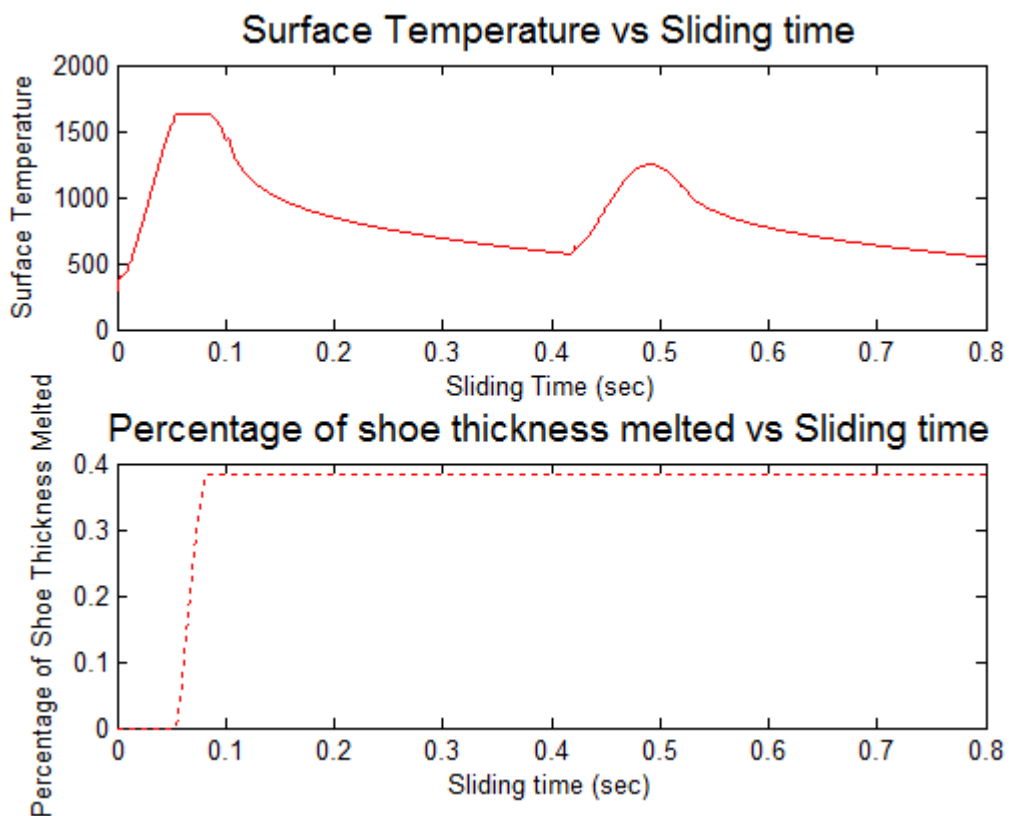


Figure 4.27: SS: Pressure 2.07 MPa, Velocity 762 m/s, Surface Temperature and % Melt vs. Time

Figure 4.27 in the top plot shows the surface temperature versus sliding time for stainless steel 304 with the lowest bearing pressure of 2.07 MPa and higher velocity of 762 m/s. The temperature profile corresponds with the sinusoidal pressure profile shown in Figure 4.21. At each point in contact the temperature begins to rise due to the frictional heat energy being generated. When it is not in contact the temperature

decreases, and at the next point in contact the temperature increases. This pattern is repeated for the duration of time. The maximum surface temperature reached 1091 K but was still below the melting temperature. As a result, no melt occurred. The trend for the high velocity cases will be that the skin temperature is elevated, and based on the bearing pressure, melt may or may not occur.



**Figure 4.28: SS: Pressure 4.14 MPa, Velocity 762 m/s, Surface Temperature and % Melt vs. Time**

Figure 4.28 in the top plot shows the surface temperature versus sliding time for stainless steel 304 with a bearing pressure of 4.14 MPa and higher velocity of 762 m/s. The temperature profile corresponds with the sinusoidal pressure profile shown in Figure

4.22. At each point in contact the temperature begins to rise due to the frictional heat energy being generated. When it is not in contact the temperature decreases, and at the next point in contact the temperature increases. This pattern is repeated for the duration of time. The maximum surface temperature reached melt at 1632 K. This is the first instance of melt in the Wolfson scenarios thus far. The percentage of total melt wear predicted is 0.38% of the total volume.

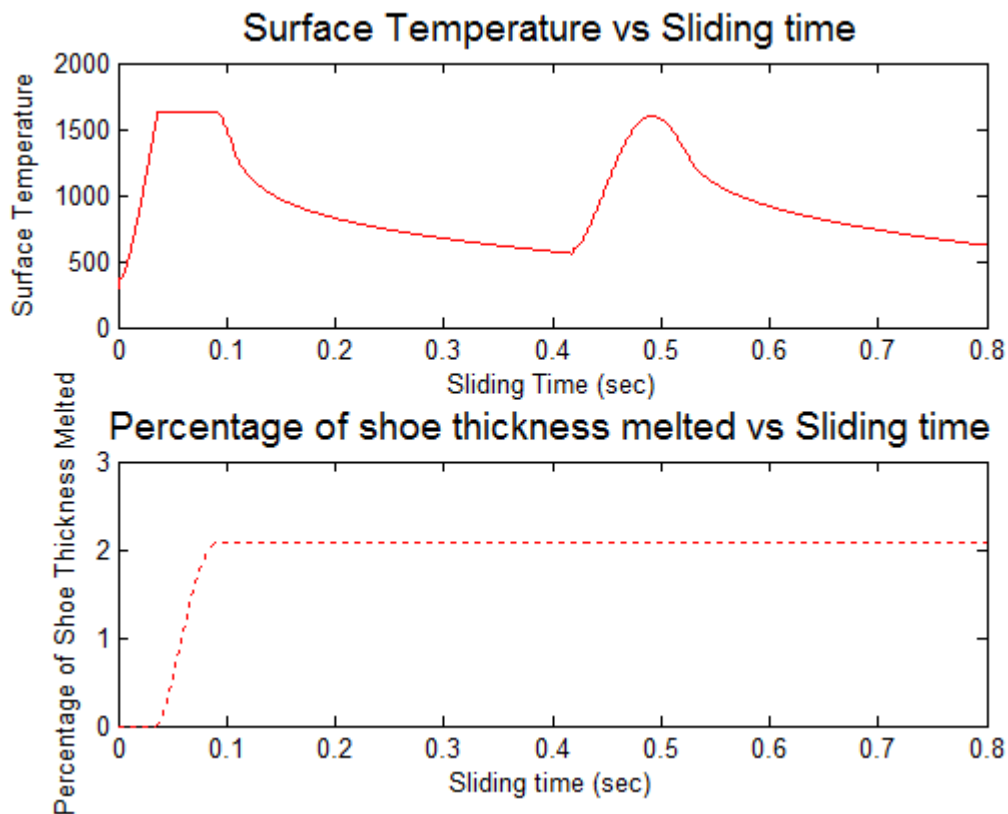


Figure 4.29: SS: Pressure 6.21 MPa, Velocity 762 m/s, Surface Temperature and % Melt vs. Time

Figure 4.29 in the top plot shows the surface temperature versus sliding time for stainless steel 304 with the highest bearing pressure of 6.21 MPa and velocity of 762 m/s.

The temperature profile corresponds with the sinusoidal pressure profile shown in Figure 4.23. At each point in contact the temperature begins to rise due to the frictional heat energy being generated. When it is not in contact the temperature decreases, and at the next point in contact the temperature increases. This pattern is repeated for the duration of time. As in the previous scenario, the maximum surface temperature also reached melt at 1632 K. The percentage of total melt wear is 2%. This is the worst-case scenario, as expected, given the highest bearing pressure and faster velocity.

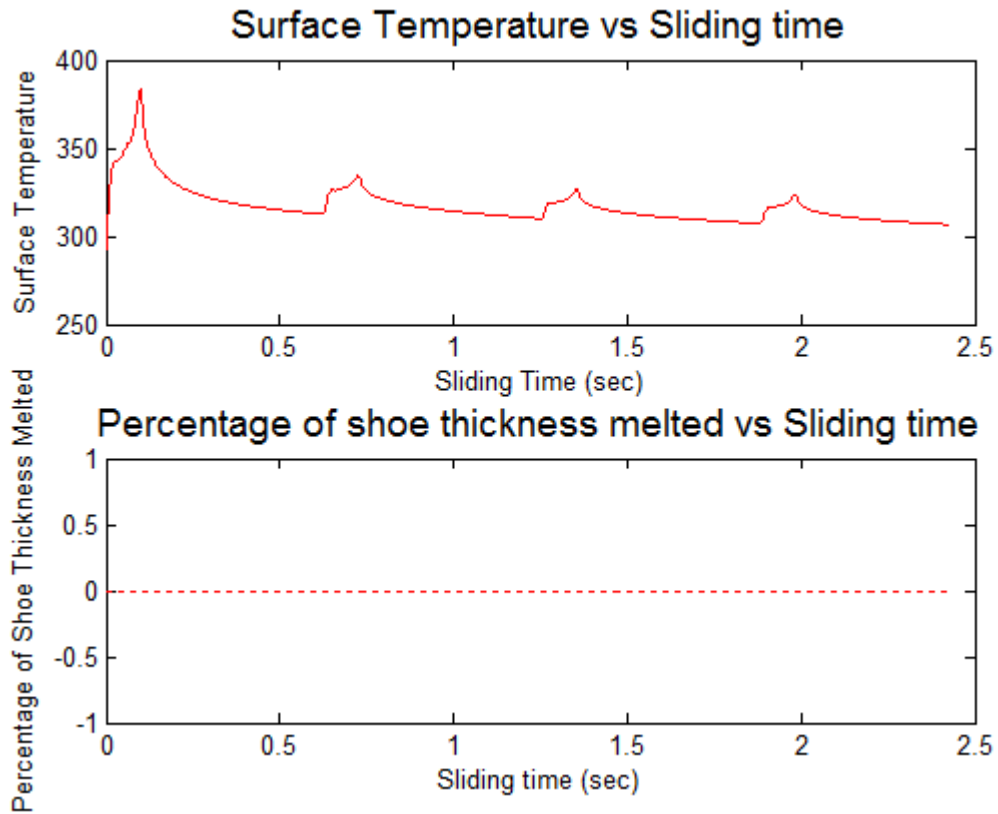
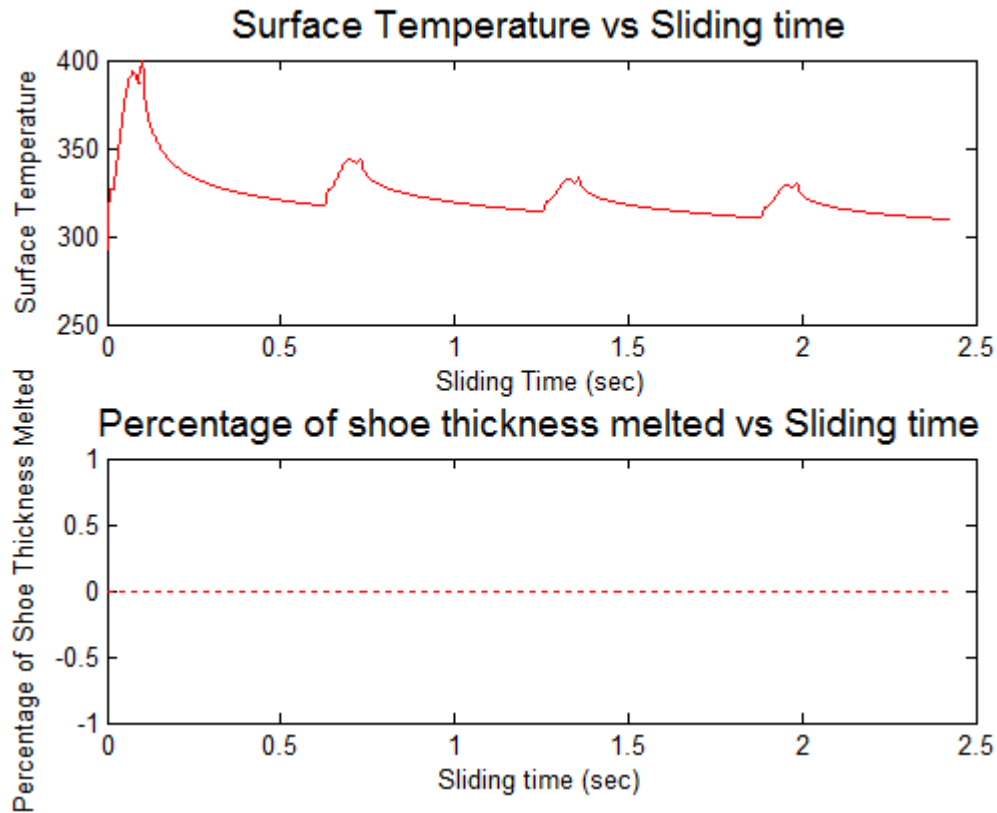


Figure 4.30: Mo: Pressure 2.07 MPa, Velocity 251 m/s, Surface Temperature and % Melt vs. Time

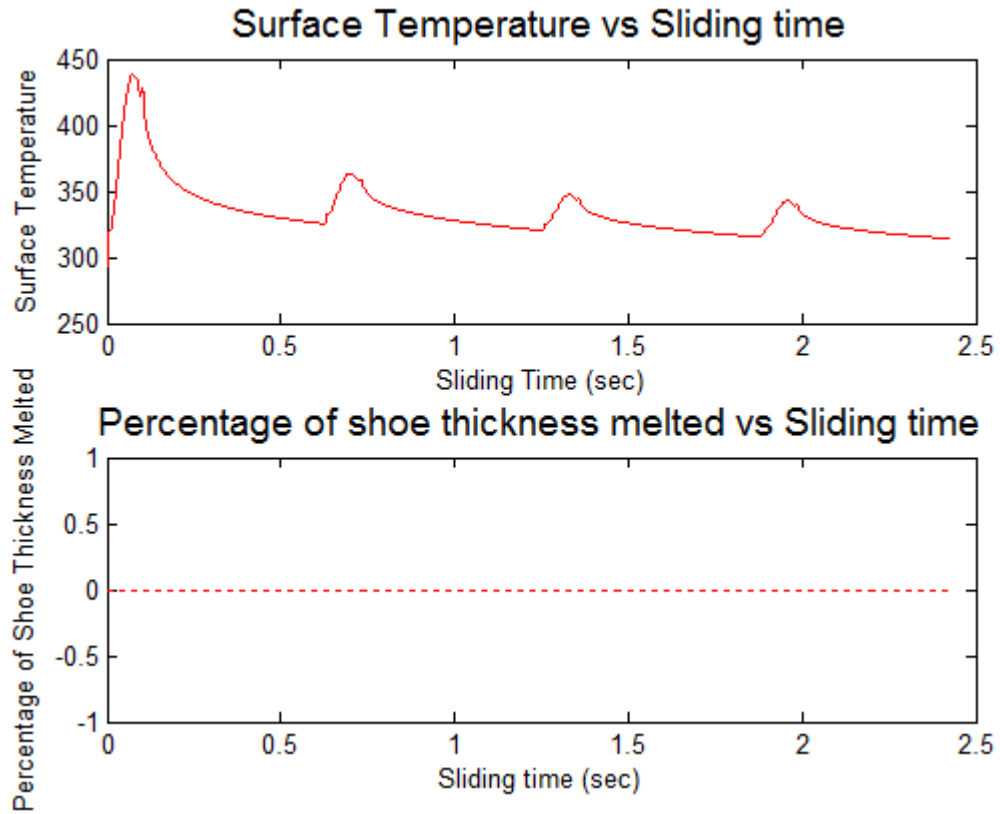
The following figures show the results from molybdenum. Given the greater melt temperature for this material at 2890 K, the resistance to melt is much higher and as a trend, the surface temperatures are lower for molybdenum than stainless steel. Figure 4.30 shows the surface temperature plotted versus sliding time with a bearing pressure of 2.07 MPa and constant velocity of 251 m/s. The maximum surface temperature reached 383 K, far below the melt temperature. As a result, no melt occurred.



**Figure 4.31: Mo: Pressure 4.14 MPa, Velocity 251 m/s, Surface Temperature and % Melt vs. Time**

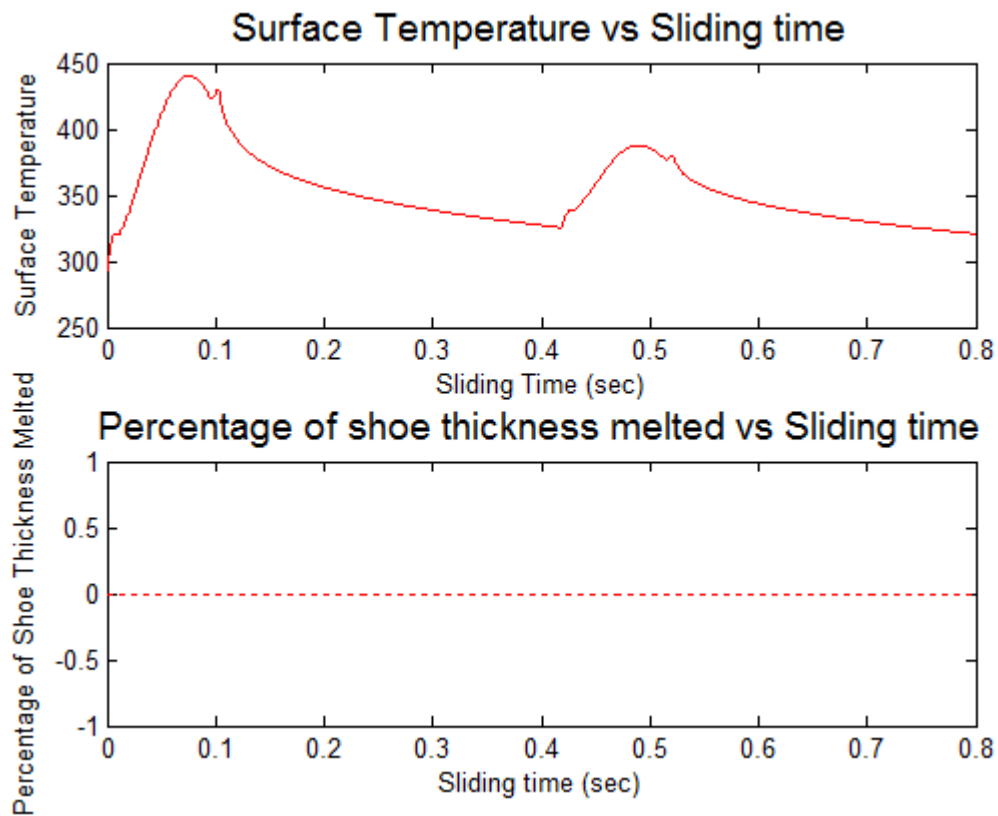
Figure 4.31 shows the surface temperature plotted versus sliding time with a bearing pressure of 4.14 MPa and constant velocity of 251 m/s. The maximum surface

temperature was well below the melt temperature for molybdenum. For this scenario, the temperature reached 399 K. As a result, no melt occurred.



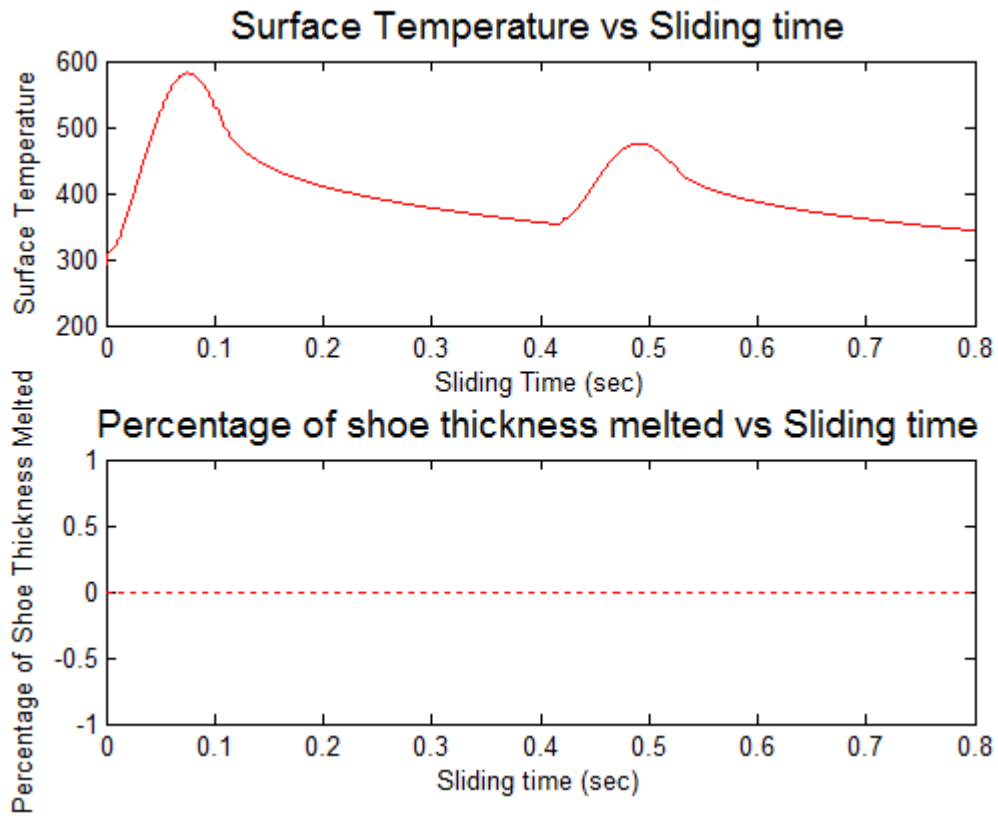
**Figure 4.32: Mo: Pressure 6.21 MPa, Velocity 251 m/s, Surface Temperature and % Melt vs. Time**

Figure 4.32 shows the surface temperature plotted versus sliding time with the highest bearing pressure of 6.21 MPa and constant velocity of 251 m/s. For this scenario, the temperature reached 438 K, still far below the melt temperature for molybdenum. As a result, no melt occurred.



**Figure 4.33: Mo: Pressure 2.07 MPa, Velocity 762 m/s, Surface Temperature and % Melt vs. Time**

The following figures show the molybdenum results for the higher velocity case. The temperatures are higher given the higher velocity; however, as stated previously, the resistance to wear is greater due to molybdenum's high melting temperature. Figure 4.33 shows the surface temperature plotted versus sliding time with a bearing pressure of 2.07 MPa and constant velocity of 762 m/s. The maximum surface temperature reached 440 K. No melt occurred.



**Figure 4.34: Mo: Pressure 4.14 MPa, Velocity 762 m/s, Surface Temperature and % Melt vs. Time**

Figure 4.34 shows the surface temperature plotted versus sliding time with a bearing pressure of 4.14 MPa and constant velocity of 762 m/s. The maximum surface temperature reached 581 K, and as a result, no melt occurred.

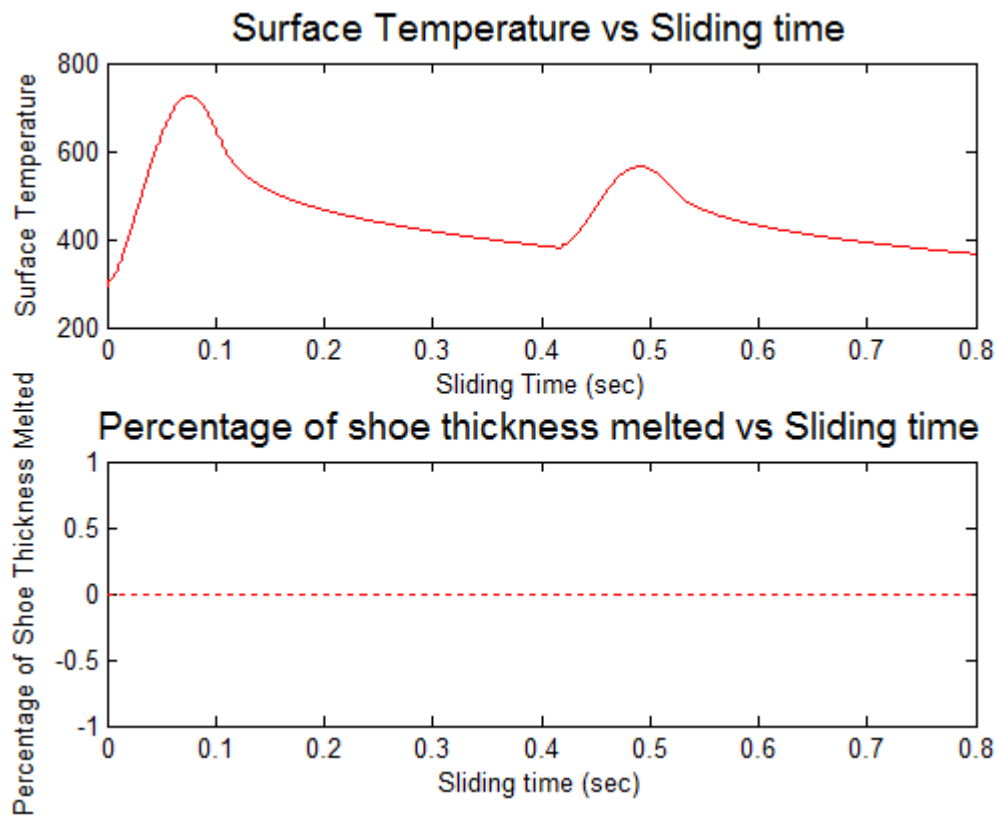


**Figure 4.35: Mo: Pressure 900 psi, Velocity 2500 ft/sec, Surface Temperature and % Melt vs. Time**

Figure 4.35 shows the surface temperature plotted versus sliding time with a bearing pressure of 6.21 MPa and constant velocity of 762 m/s. This is the worst case scenario for molybdenum; however, the maximum surface temperature reached 724 K, still a considerable amount below the melting temperature. No melt occurred in any of the molybdenum scenarios.

After analyzing the results above, they agree with Wolfson's conclusions in 1960. Wolfson indicated the wear rate of stainless steel increases with velocity at pressures above 2.07 MPa (300 psi) [11]. The results in Figures 4.24 to 4.29 agree with his conclusions; the increased skin temperature in these figures indicates that wear is more

likely to occur given the high pressure and velocity. Wolfson also made the conclusion that there was no major difference in the wear rates of molybdenum when tested at 251 m/s (850 ft/s) and 762 m/s (2500 ft/s) and subjected to the different bearing pressures [11]. The results shown in Figures 4.30 to 4.35 agree with his conclusion in that molybdenum did not reach melt in any scenario, and the average temperatures remained below 500 K.

The next section describes the HHSTT test utilizing the DADS data, Montgomery coefficient of friction, and the same methodology that was carried out in Wolfson's experiments. The major difference between Wolfson and the HHSTT is that the former tested constant velocity and constant pressure, whereas the HHSTT scenario is time dependent in both. Furthermore, the pressure profile for Wolfson's was modified to incorporate the bounce condition with a sinusoidal function that indicated when in contact and when not in contact. This was done to compare the results based on the known bounce phenomenon in the HHSTT test.

#### **4.2 A More Physics-Based Approach to the Partition Function**

The partition function that was used to compare the Wolfson experiment to the HHSTT scenario was evaluated based on a mathematical approach. It is arbitrary in nature and purely hypothesized. This section describes a more physics-based approach to the partition function.

There are two assumptions in this analysis. The first applies to the Wolfson experiment by assuming constant contact, constant velocity, and zero acceleration. Initially, half of the total frictional heat energy is dissipated into the shoe, i.e.  $\alpha_0 = 0.5$  and

linearly decreases to a minimum value  $\alpha_m$ , which is defined as the partition value at melt. There is a defined time to melt,  $t_m$ , which is the time to reach the material's melting point at the slipper-to-rail interface. This time is a function of the material properties of the slipper made of VascoMax 300:  $T_m$ , melt temperature,  $k$ , thermal conductivity,  $\kappa$ , thermal diffusivity,  $\alpha$ , the average of  $\alpha_0$  and  $\alpha_m$ ,  $\mu$ , the coefficient of friction,  $P$ , the average contact pressure, and  $v_0$ , the constant velocity. It is also a function of the ambient temperature  $T_0$ . The mathematical equation for  $t_m$  is defined in Equation 4.27 [11].

$$t_m = \frac{\pi}{k} \left( \frac{(T_m - T_0)\kappa}{2\mu\alpha P v_0} \right)^2 \quad (4.27)$$

This equation is equivalent to solving  $T_1(0, t_m) = T_m$  for  $t_m$ . At  $t_m$ , the partition function asymptotes to a straight line at  $\alpha_m$ . Here the value for  $\alpha_m$  is set to 0.1 which was the case for the exponential decay function. This value is reasonable because the percentage of heat energy entering the slipper diminishes over time. By including the bounce condition the time to melt is actually extended by a constant times  $t_m$ . It takes longer for the material to reach melt with bounce due to the cooling factor that takes place when the slipper is not in contact with the rail. This constant is defined as the reciprocal of frequency of contact. The percent of contact for the HHSTT test varies at different velocities as shown in Figure 4.36.

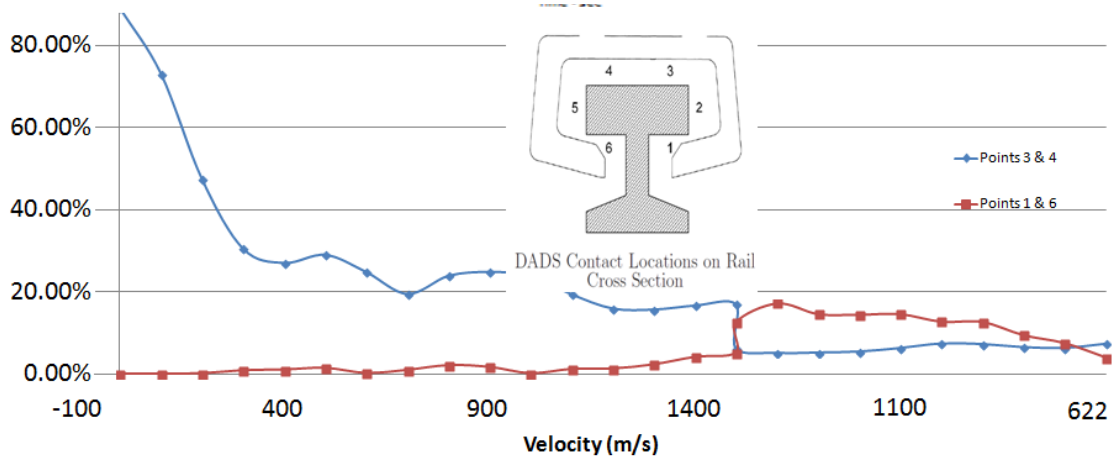
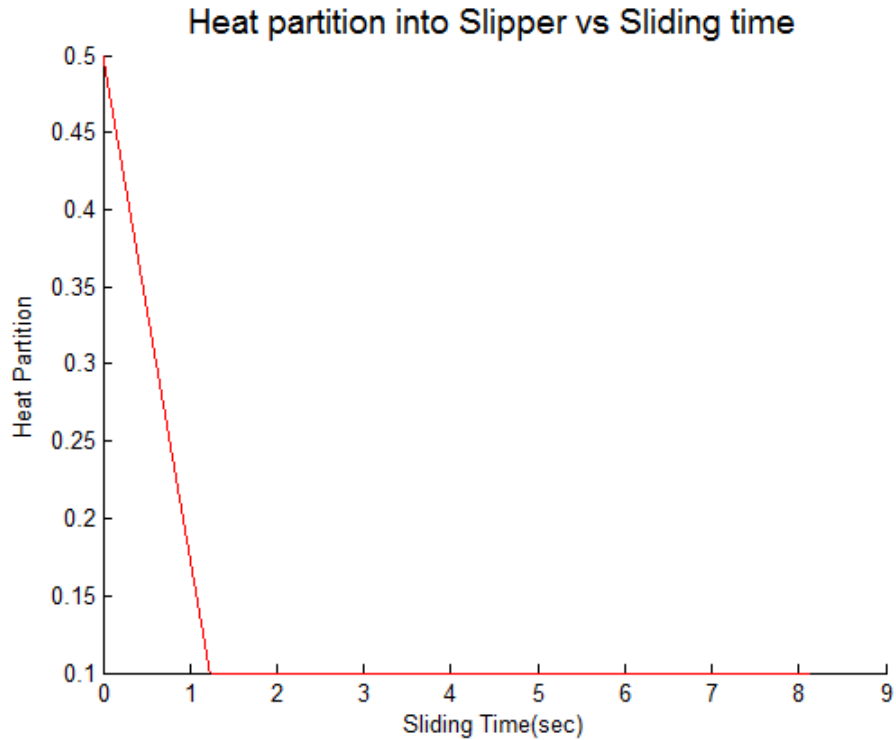


Figure 4.36: Percent Contact vs. Velocity [1]

By taking the average of the percentages above at different velocity “windows,” the value is 22.5%. Therefore, as defined previously, the constant is  $1/0.225$  or roughly 4.44. The partition function is a bi-linear function that begins at  $\alpha_0$  and linearly decreases to  $\alpha_m$  at the adjusted melt time based on the frequency of contact. Mathematically the partition is a piecewise equation described in Equation 4.28.

$$\alpha(t) = \begin{cases} \alpha_0 + (\alpha_m - \alpha_0) \frac{t - t_0}{\text{constant} \cdot t_m - t_0} & \text{for } t < \text{constant} \cdot t_m \\ \alpha_m & \text{for } t > \text{constant} \cdot t_m \end{cases} \quad (4.28)$$

The plot for this function is shown in Figure 4.37.



**Figure 4.37: Bilinear Partition Function vs. Time (Equation 4.28)**

Next, consider the second assumption of increasing velocity and nonzero acceleration where  $a \neq 0$ . This assumption agrees with the HHSTT scenario where velocity is a function of time, and the initial velocity is zero. For this case the time to melt,  $t_m$  is defined as the square of  $s$  where  $s$  is solved by the following equations [11].

$$s^3 + \beta s - \lambda = 0,$$

where  $\beta = \frac{3q_0}{a}$  and  $\lambda = \frac{3T_m \kappa}{2\alpha Pa} \sqrt{\frac{\pi}{k}} \frac{1}{\mu}$  (4.29)

The exact solution to Equation 4.29 is shown below in Equation 4.30.

$$s = \left(\frac{\lambda}{2}\right)^{1/3} \left[ (\sqrt{1+M} + 1)^{1/3} - (\sqrt{1+M} - 1)^{1/3} \right] \quad \text{where } M = \frac{4\beta^3}{27\lambda^2}$$

(4.30)

The acceleration is 305.9 m/sec<sup>2</sup> which is the average of each of the increasing linear slopes of the velocity curve shown in Figure 4.38. Furthermore, the initial velocity is zero because the slipper begins at rest.

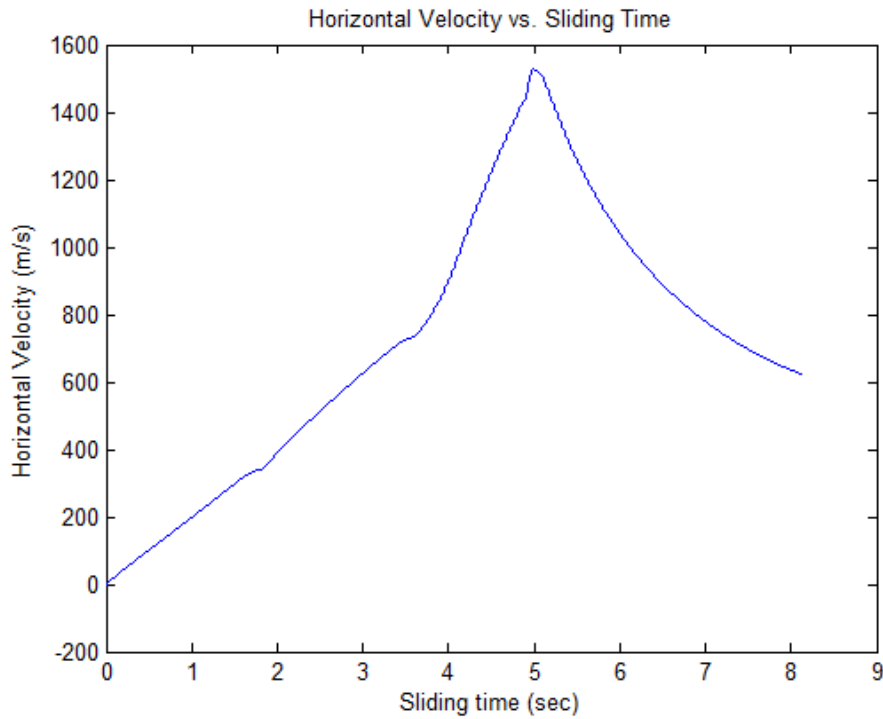
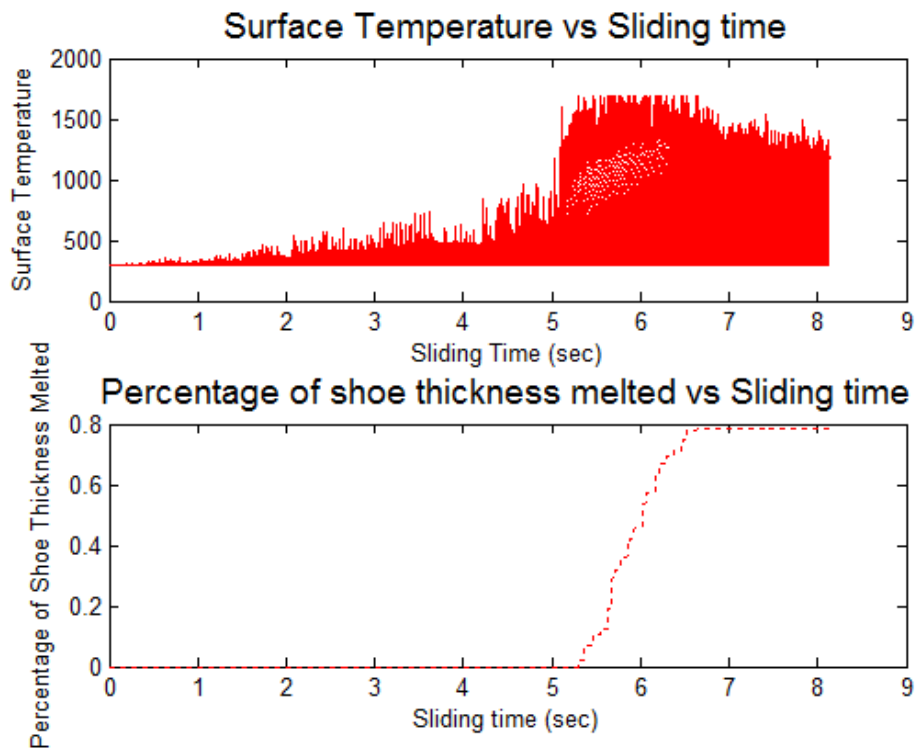


Figure 4.38: Horizontal Velocity vs. Time

For the constant acceleration assumption different methods of characterizing the partition function were examined to model the heat flow into the slipper based on physical rationale. The previous partition function assumed a mathematical formulation of an exponential decay function. The same initial conditions apply where  $\alpha_0 = 0.5$  which assumes that half of the heat flow goes into the slipper. Recall that Figure 3.9 showed the partition function versus time plot. As a result the temperature distribution is shown in Figure 4.39. From the heat transfer analysis described in the previous chapter, the total melt wear based on this exponential function resulted in 0.787% of the total slipper volume.



**Figure 4.39: Surface Temperature and Melt Wear Percentage vs. Sliding Time Using Exponential Partition Function**

The next partition function considered is a bilinear decay function described in Equation 4.31.

$$\alpha(t) = \begin{cases} \alpha_0 + (\alpha_m - \alpha_0) \frac{t}{\text{constant} \cdot t_m} & \text{for } t < \text{constant} \cdot t_m \\ \alpha_m & \text{for } t > \text{constant} \cdot t_m \end{cases} \quad (4.31)$$

It is of the same form as the previous equation described under the assumption of constant velocity. By including the bounce condition, the time to melt under the assumption of constant acceleration is about 5 seconds. This time is longer than the results found from the constant velocity assumption, which is expected because with bounce there is a cooling factor that takes place when the slipper is not in contact with the rail. Therefore, the time to reach melt is extended. The plot of the partition function is shown in Figure 4.40.

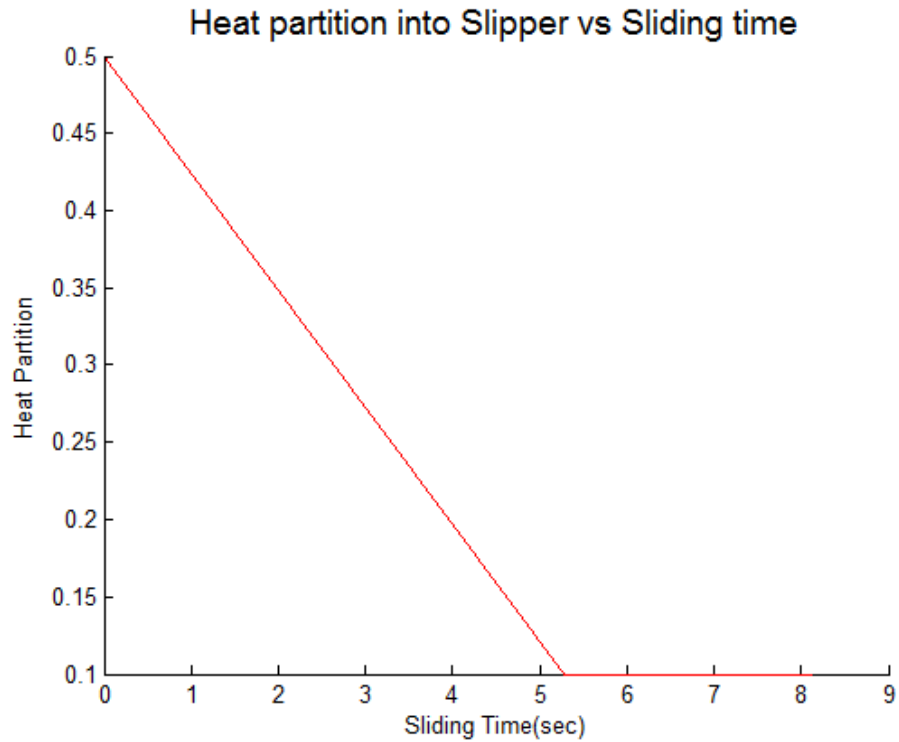


**Figure 4.40: Bilinear Partition Function vs. Time (Equation 4.31)**

The initial condition  $\alpha_0$  remains at 0.5 and equilibrates to a lower value of 0.1. The simplest method of conjoining the two points is by a straight line. Based on this partition function, Figure 4.41 shows the temperature distribution over time. The total melt wear predicted was 3.39%. This is an overestimation relative to the exponential decay function, which predicted 0.78%.

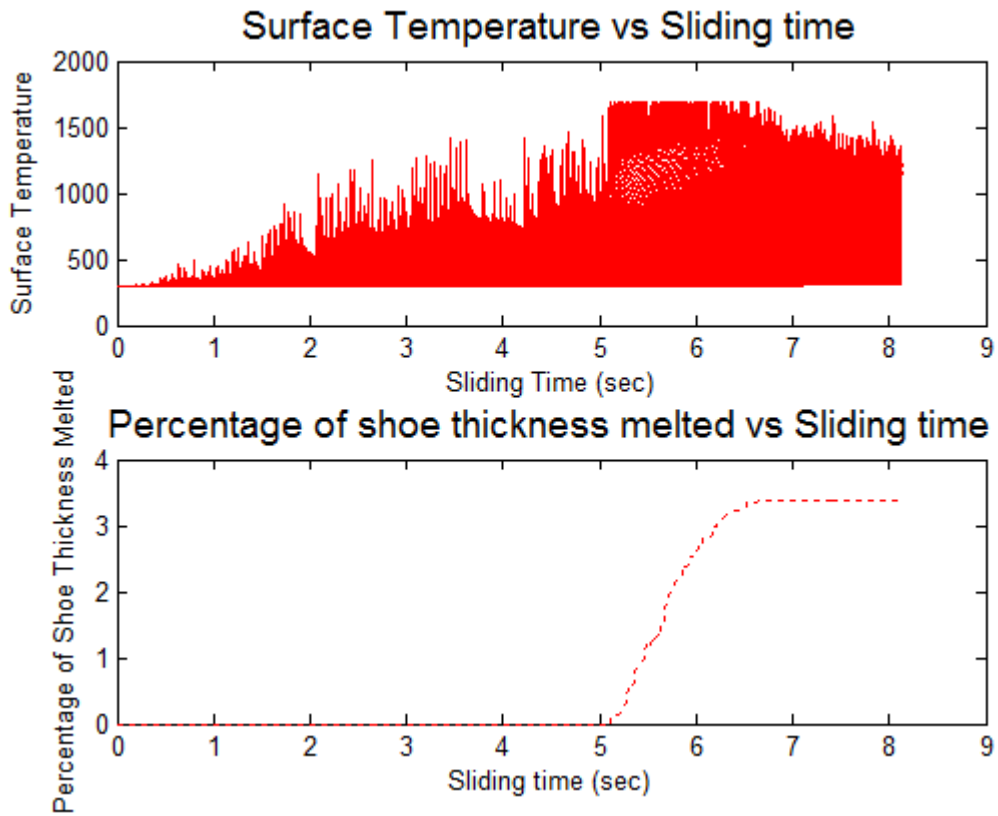


**Figure 4.41: Surface Temperature and Melt Wear Percentage vs. Sliding Time Using Bilinear Partition Function**

The next partition function is based on the same  $\alpha_0$  and  $\alpha_m$  values, but rather than the linear behavior of the function when  $t < t_m$ , this function behaves as an exponential decay. The assumed formula for the function is given in Equation 4.32.

$$\alpha(t) = \alpha_0 e^{-\beta t} \quad \text{for } t < \text{constant} \cdot t_m \quad (4.32)$$

$\beta$  is the rate of decay and is derived by substituting  $t_m$  for  $t$ . The relationship is shown in Equation 4.33.

$$\alpha(t_m) = \alpha_0 e^{-\beta t_m} \quad (4.33)$$

Solving for  $\beta$  in Equation 4.33 yields the following

$$\beta = -\frac{1}{t_m} \ln\left(\frac{\alpha_m}{\alpha_0}\right) \quad (4.34)$$

By substituting Equation 4.34 back into Equation 4.33, it yields the power form of the partition function shown in Equation 4.35.

$$\alpha(t) = \begin{cases} \alpha_0 \left(\frac{\alpha_m}{\alpha_0}\right)^{\frac{t}{\text{constant} \cdot t_m}} & \text{for } t < \text{constant} \cdot t_m \\ \alpha_m & \text{for } t > \text{constant} \cdot t_m \end{cases} \quad (4.35)$$

From Figure 4.42, the behavior of the function for  $t < t_m$  is at rate defined by Equation 4.35.

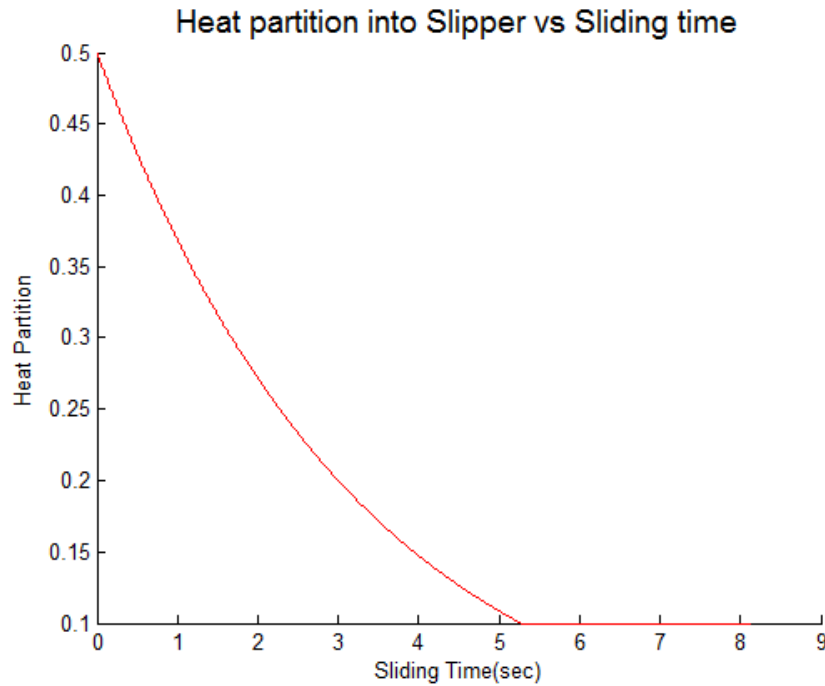


**Figure 4.42: Power Partition Function vs. Time (Equation 4.35)**

Figure 4.43 shows the temperature distribution based on this partition function. The total melt wear predicted with this partition function is 2.09%. This is less than the predicted melt wear compared to the linear function but is still an overestimation.

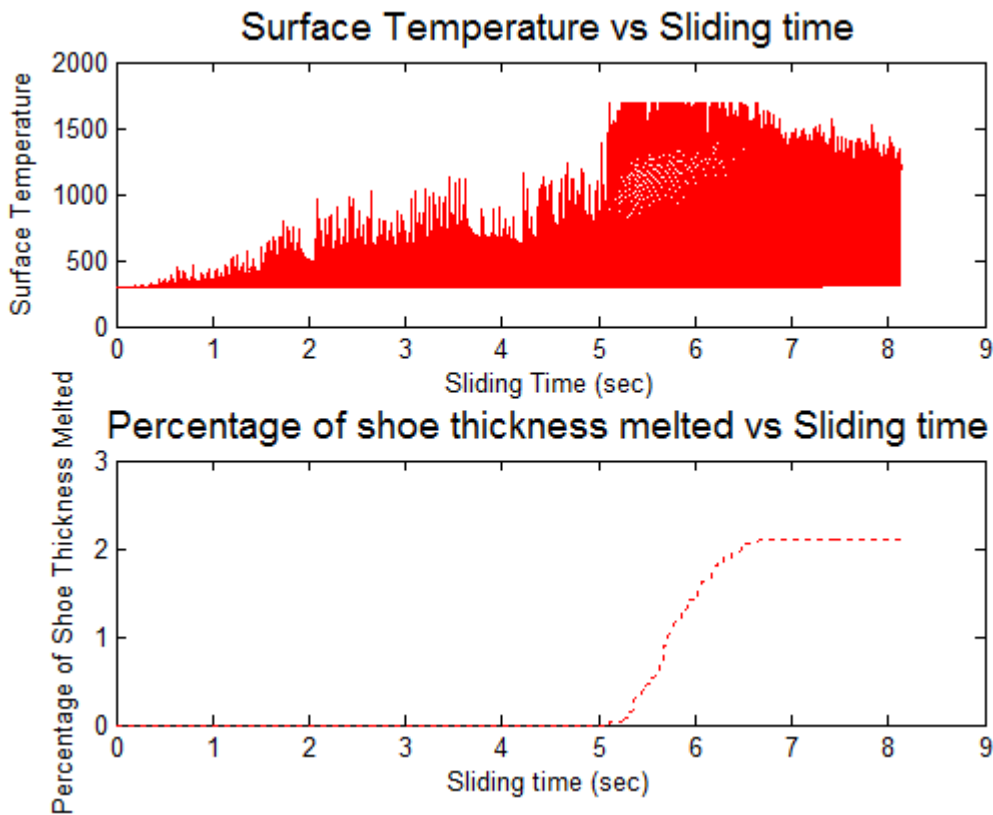


**Figure 4.43: Surface Temperature and Melt Wear Percentage vs. Sliding Time Using Power Partition Function**

The next partition function takes the same formulation as the powered function but now the exponent is squared. The rationale behind squaring the powered term is that it behaves as a decaying function but fits the Gaussian distribution. Equation 4.36 describes this function and note the squared term in the exponent.

$$\alpha(t) = \begin{cases} \alpha_0 \left( \frac{\alpha_m}{\alpha_0} \right)^{\left( \frac{t}{\text{constant} \cdot t_m} \right)^2} & \text{for } t < \text{constant} \cdot t_m \\ \alpha_m & \text{for } t > \text{constant} \cdot t_m \end{cases} \quad (4.36)$$

Thus far the three partition functions each give a predicted total melt wear percentage based on the behavior of the partition function. It is apparent that the behavior for  $t < t_m$  drives the solution for total melt wear. The fourth function as shown in Equation 4.36 is the final assumed formula for describing the heat flow into the slipper. It was hypothesized that the function would fall somewhere between the first exponential decay function and the power function. However, by squaring the exponent it drives the early on heat flow into the slipper. The behavior of the partition function is shown in Figure 4.44.

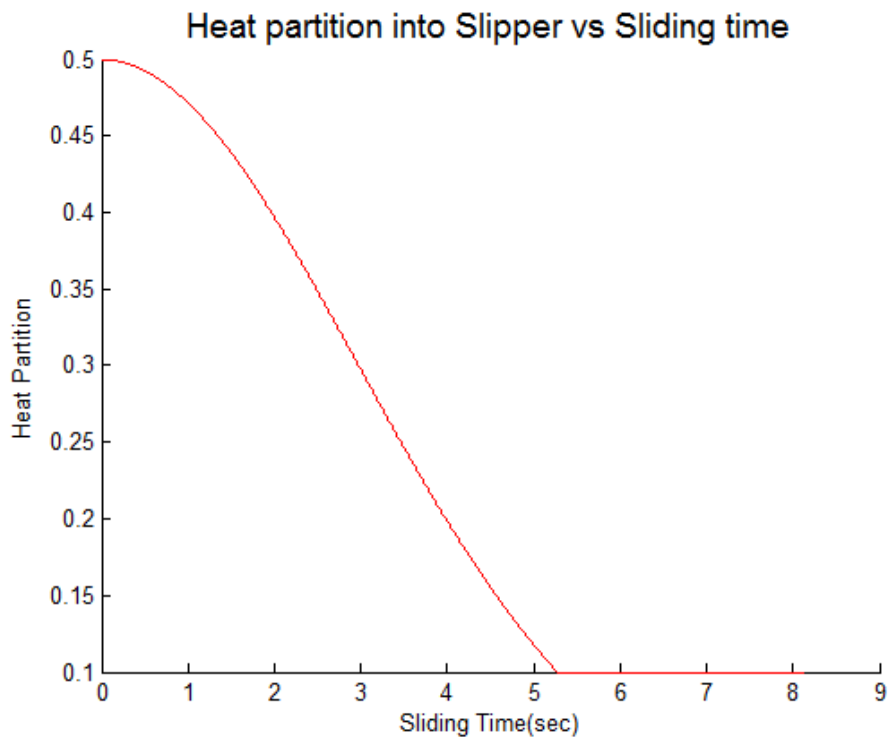


**Figure 4.44: Power Squared Partition Function vs. Time (Equation 4.36)**

The results of squaring the exponent are shown in Figure 4.45 which shows higher surface temperatures and a greater melt wear percentage overall. The predicted total melt wear is 3.61%.

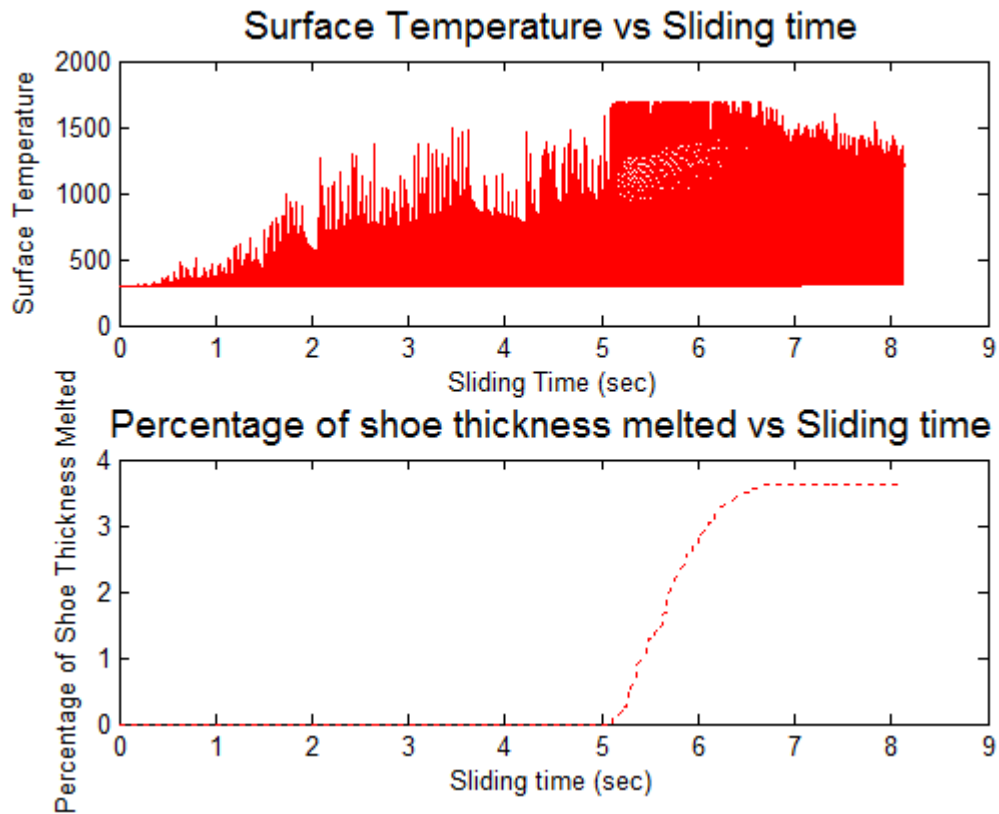


**Figure 4.45: Surface Temperature and Melt Wear Percentage vs. Sliding Time Using Power Squared Partition Function**

All four partition functions described in this chapter are an assumed formula to describe how the heat is partitioned between the slipper and rail as time goes on. Given the assumed formula and by computing the heat transfer analysis via the MATLAB code described in Chapter 3, the solution of total melt wear is predicted based on some rationale. The rationale behind the first partition function is that it provided a reasonable solution to total melt wear. The other three functions are motivated by the physics of the

problem by incorporating the DADS data to determine the melt time. A comparison of each partition function is shown in Figure 4.46.

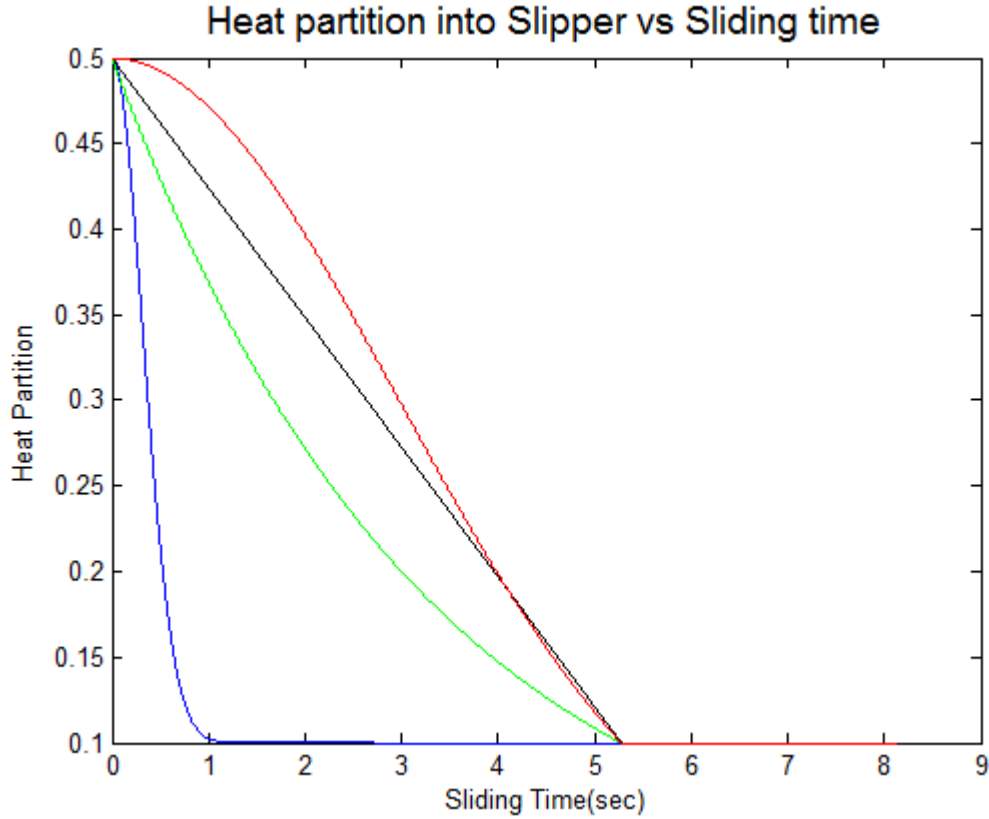


**Figure 4.46: Comparison of All Partition Functions vs. Time**

The results of each partition function and predicted melt wear is summarized here.

The function with the fastest decay rate is  $\alpha(t) = 0.4e^{-5t^2} + 0.1$  represented by the blue curve and the predicted melt wear is 0.79%. The next function is the bilinear equation represented by the black curve, and the predicted melt wear is 3.39%. This overestimation of melt wear led to next assumed solution in which  $t < t_m$  behaves as a

power function written as  $\alpha(t) = \alpha_0 \left( \frac{\alpha_m}{\alpha_0} \right)^{\frac{t}{\text{constant} * t_m}}$  and shown in the green curve. Using

this formula the predicted total melt wear is 2.06%. Finally, the power function was

modified to  $\alpha(t) = \alpha_0 \left( \frac{\alpha_m}{\alpha_0} \right)^{\left( \frac{t}{\text{constant} * t_m} \right)^2}$  as shown by the red curve and resulted in a

prediction of 3.61% melt wear.

## V. Conclusions and Recommendations

### 5.1 Summary

The research presented in this thesis is an evaluation of thermal environment developed by a slipper traveling at high velocity on a stationary rail. The thermal analysis is a one-dimensional approach that incorporates heat conduction when the slipper and rail are in contact, heat convection when not in contact, and the latent heat of fusion at the onset of melt. Due to the contact forces between the slipper and rail, frictional energy is generated. The energy is then converted to heat which results in a thermal environment that is truly three-dimensional. In an effort to simplify the problem, the present research used a one-dimensional approach by considering the heat flow into the slipper. This approximation was based on a partition function that separates the flow field between the slipper and the rail. Specific conclusions about this research work are discussed in this section.

### 5.2 Conclusions

The Wolfson scenarios showed that stainless steel was more susceptible to melt wear as compared to molybdenum. This indicates that the resistance to wear is a function of material properties such as melt temperature and thermal conductivity. The Wolfson

scenarios also showed that the wear rate of stainless steel increases with high velocity and bearing pressures above 2.07 MPa. This conclusion leads to the HHSTT test where the pressures reach in excess of 6.21 MPa, which was the highest bearing pressure in all the Wolfson scenarios.

Several conclusions are drawn from the research work that involved the HHSTT test. Overall, the wear phenomenon is a three-dimensional problem, and in this research, it has been simplified to a one-dimensional approach. This assumption led to determining the behavior of the partition function. The partition function is used to separate the heat flow into the slipper. By characterizing the function in different ways it can be concluded that there are sensitivity issues with the formulation of the function. For example, the exponential function yielded the lowest percentage of melt wear at 0.79%. This was considered the baseline, because the function was fit to match actual metallurgy results of the recovered slipper. It was estimated that the slipper wore less than 1% of its total volume; therefore this  $\alpha(t)$  is the closest representation of reality. The highest predicted melt wear was 3.6% using a different approach. Based on each equation the sensitivity lies in the decay rate of the function. The faster the function decays, the less overall melt wear predicted. Furthermore, the exponential formulation was based on the assumption that the slipper was in contact with the rail at all times and resulted in reaching melt faster. By incorporating the bounce condition, the time to melt is actually increased by a constant factor. One can also conclude that the total melt wear predicted is an overestimation of the actual value. This is based on the assumption that there is no surface thermal loss when not in contact. In reality, there is convective heat loss that takes place. Another conclusion is that the partition functions described in this

research are motivated by physics and provides a rationale to how the function is defined. The difficulty lies in determining the actual formulation of the function and at this time is still an unknown. However, given the experimental data provided in DADS and the qualitative analysis performed in this research, the results are in general agreement with wear theory and provide useful information for future research endeavors.

### **5.3 Significance of Research**

The significance of this research is found in the formulation of the partition function. Previous work had assumed this value to be constant which is inappropriate for modeling the time-dependent events of the HHSTT scenario. The other approach to modeling the partition function was merely hypothesized to fit the results from the recovered slipper. This function was arbitrary in nature and related the known melt wear to a mathematical formulation. It also assumed 100% contact between the slipper and the rail, and that is known to be artificial. The other partition functions were motivated by the physics of the problem. It was rationalized that the time to melt should be extended given the bounce condition. This was factored into the scenario by constant multiplier that was solved for by taking the reciprocal of the frequency of contact. This extended the time to melt to about 5 seconds. With the culmination of this research and the work of others, it is understood that temperature has a great effect on the wear phenomenon. The partition function plays a big role in determining the temperature profile of the slipper but has not yet been completely defined. This research has taken the methodology of how it should behave and is the closest to determining an actual partition function.

#### **5.4 Recommendations for Future Research**

The approach to understanding the melt wear phenomenon has been simplified to a one-dimensional analysis of heat transfer. This is useful to eliminate complexities yet still provides a reasonable solution. The next step in this research endeavor is to completely define the partition function as it drives the overall analysis to determining melt wear. Future research should examine the partition function with respect to time as well as temperature. Further\ efforts should be made in determining a more realistic heat convection coefficient. The coefficient should be a value much higher than what is currently assumed given the high velocities in the HHSTT test. Also the thermal conductivity of steel in some instances is found to be a function of temperature. Research in this area would be beneficial to refine the analysis presented here. Another consideration for future research is the modification of the upper boundary condition in the heat transfer analysis. This condition can be modeled as convection just as the lower boundary is considered when not in contact. In addition to melt wear, the total wear includes mechanical wear which is the amount of material removed due to asperities on the rail. This has been modeled using a two-dimensional plane strain failure criteria by Johnson and Cook [3]. This research did not address the mechanical wear but has shown that the thermal environment greatly affects the total wear of the slipper. Developments of further wear theory include the culmination of both mechanical and melt wear.

## Appendix A. DADS Data in MATLAB Code

### A.1 MATLAB Code Description

This MATLAB script file takes the DADS data and loads it into a MATLAB readable file. It creates variables for time, velocity, and force and saves the variables to a file for use in the subsequent MATLAB program.

### A.2 DADS Data File Extraction MATLAB Code

```
%% DADS Jan2008 data conversion
%
%   Maj Chad Hale, PhD-09S
%
%   Extracts variables from Jan 2008 DADS data file (DADS_Jan2008.mat)
%   provided by George Ayers on 20 Jan 2009.
%

clear; clc;
close all
format short

% load the data file
load DADS_Jan2008_alldata_refined           % includes 4th stage 80XG1
velocity profile data
%load DADS_Jan2008_alldata                 % includes 4th stage 80XG1
velocity profile data
%% extract the variables for later DADS statistical analysis

% DADS analysis time array
time = DADS_Jan2008_noheader_alldata_refined(:,1);

% sled center of gravity position data
cg_horiz = DADS_Jan2008_noheader_alldata_refined(:,4);
cg_lat = DADS_Jan2008_noheader_alldata_refined(:,2);
cg_vert = DADS_Jan2008_noheader_alldata_refined(:,3);

% sled center of gravity velocity data
vsled_horiz = DADS_Jan2008_noheader_alldata_refined(:,7);
vsled_lat = DADS_Jan2008_noheader_alldata_refined(:,5);
vsled_vert = DADS_Jan2008_noheader_alldata_refined(:,6);

vv_fr = DADS_Jan2008_noheader_alldata_refined(:,24);
vv_fl = DADS_Jan2008_noheader_alldata_refined(:,27);
vv_ar = DADS_Jan2008_noheader_alldata_refined(:,30);
vv_al = DADS_Jan2008_noheader_alldata_refined(:,33);

% front right slipper contact forces
f_fr1 = DADS_Jan2008_noheader_alldata_refined(:,34);
f_fr3 = DADS_Jan2008_noheader_alldata_refined(:,36);
```

```

f_fr4 = DADS_Jan2008_noheader_alldata_refined(:,37);
f_fr6 = DADS_Jan2008_noheader_alldata_refined(:,38);

% front left slipper contact forces
f_fl1 = DADS_Jan2008_noheader_alldata_refined(:,39);
f_fl3 = DADS_Jan2008_noheader_alldata_refined(:,40);
f_fl4 = DADS_Jan2008_noheader_alldata_refined(:,41);
f_fl6 = DADS_Jan2008_noheader_alldata_refined(:,43);

% aft right slipper contact forces
f_ar1 = DADS_Jan2008_noheader_alldata_refined(:,44);
f_ar3 = DADS_Jan2008_noheader_alldata_refined(:,46);
f_ar4 = DADS_Jan2008_noheader_alldata_refined(:,47);
f_ar6 = DADS_Jan2008_noheader_alldata_refined(:,48);

% aft left slipper contact forces
f_al1 = DADS_Jan2008_noheader_alldata_refined(:,49);
f_al3 = DADS_Jan2008_noheader_alldata_refined(:,50);
f_al4 = DADS_Jan2008_noheader_alldata_refined(:,51);
f_al6 = DADS_Jan2008_noheader_alldata_refined(:,53);

%% additional parameters to print
cgaccel_lat = DADS_Jan2008_noheader_alldata_refined(:,8);
cgaccel_vert = DADS_Jan2008_noheader_alldata_refined(:,9);
cgaccel_horiz = DADS_Jan2008_noheader_alldata_refined(:,10);

save DADS_Jan2008_refined_FixVerticalVelocity
disp('Saving variables to ''DADS_Jan2008_refined.mat''. Finished with
data extraction....')

% return

```

## Appendix B. Heat Transfer MATLAB Code

```
% ONE-DIMENSIONAL SLIPPER TEMPERATURE GRADIENT ANALYSIS
% Original Finite Difference Code Written by Capt. Greg Cameron, MS-06.
% Adapted for DADS Analysis by LtCol Chad Hale, PhD-09.
% Modified by Stephen Meador, MS-10.
% Modified by Jacob Goldberg, PhD-10.
% Modified by Alexis Hurst, MS-11.
% Modified by Gracie Paek-Spidell, PhD-11.
% Modified by Kathleen Le, MS-13.

tic
close all; clc;
global Km Kr r z time Tmelt Tinit v_xi_t sigma thickness SlipPartition
melt_wear cg_horiz
%%
% Load Data
dataDADS = load('DADS_Jan2008_alldata_refined');

time = DADS_Jan2008_noheader_alldata_refined(:,1);           %
(sec)
cg_horiz = DADS_Jan2008_noheader_alldata_refined(:,4)*.0254; %
horizontal distance , (m)
vsled_horiz = DADS_Jan2008_noheader_alldata_refined(:,7)*.0254; %
horizontal velocity (m/s)
% vsled_horiz = 500;
% cg_horiz = 609.6;
% vsled_horiz = 251;

%%
% Set Material Constants
Cp_air = 1004; % specific heat, J/(kg K) for 298K
nu_air = 15.7e-6;
Cp_He = 5193; % specific heat, J/(kg K) for 298K
nu_He = 122.237e-6;
D_HeBag = 1310; % distance in meters from initial position
to start of He bag
Tinit = 293; % initial temperature, K

% Set Slipper Constants
slideCont = 1/1; % percentage of slipper in contact while
sliding
Sw = 4*0.0254; % slipper width, m
Sl = 8*0.0254; % slipper length, m
An = Sw*Sl; % slipper area, m^2 ( = 32 sq in)
thickness = 14.7E-3; % slipper thickness, m (14.7 mm)
vol = An * thickness; % slipper "plate" volume, m^3
rho_V300 = 8000; % density, kg/m^3
mass = rho_V300 * vol; % single slipper mass, kg
Cp_V300 = 420; % specific heat, J/(kg K)...at 700K (see
6Jun09, cont#3 notes)
% this is the Cp value that Laird used
numslippers = 4; % number of slippers in the sled
Tmelt = 1685; % V300 melt temperature
```

```

Km = 31; % thermal conductivity of slipper, J/(m s
K)=W/(mK)
Kr = 15; % thermal conductivity of rail,(stainless
steels)
alpha = Km/(rho_V300 * Cp_V300); % thermal diffusivity of metal,
m^2/s (formerly known as 'a')

H_VM300 = 2e9; % Slipper Hardness (Pa)

%%
% Original Code Written by Gracie Paek-Spidell, Ph.D Advanced
Candadicy, PhD-11.
% Analytical solution to partion function
% Function code in separate .m file alpha2.m
% alp2=alpha2(r,z);

%%
% Different Partitioning Functions
% SlipPartition = alp2; % heat partition going into the slipper
% (1) Exponential Function
SlipPartition = exp((-time.^2)*5)*.4+.1;
% (2) Constant contact, constant velocity, for Wolfson comparison
Pavg = 2.275e6;
% part_0 = .5;
% part_m = .1;
partition = (part_0+part_m)/2;
% v0 = 251; % Wolfson low velocity
% v0 = 762; % Wolfson high velocity
% tm = pi/k*((Tmelt-Tinit)*kappa/(2*mu*partition*Pavg*v0))^2;
percentcontact = .225; % from Dr. Baker
constant = 1/percentcontact;
% for j = 1:size(time);
%     if time(j) < constant*tm
%         SlipPartition(j) = part_0+(part_m-
part_0)*time(j)/(constant*tm);
%     else time(j) > constant*tm
%         SlipPartition(j) = part_m;
%     end
% end

% (3) Constant acceleration, zero initial velocity
v0 = 0;
accel = 305.956343; % m/s^2, or 500?
% accel = 500; %accel required to reach Mach 10 in 6 sec
lambda = 3*(Tmelt-
Tinit)*kappa/(2*partition*Pavg*accel)*sqrt(pi/k)*1/mu;
beta = 3*v0/accel;
M = 4*beta^3/(27*lambda^2);
s = (lambda/2)^(1/3)*((sqrt(1+M)+1)^(1/3)-(sqrt(1+M)-1)^(1/3));
tm = s^2;
constant = 1/percentcontact;
for j = 1:size(time);
    if time(j) < constant*tm

```

```

%      SlipPartition(j) = part_0+(part_m-
part_0)*(time(j)/(constant*tm));
      SlipPartition(j) =
part_0*(part_m/part_0)^(time(j)/(constant*tm));
%      SlipPartition(j) =
part_0*(part_m/part_0)^((time(j)^2/(constant*tm)^2));
      else time(j) > constant*tm
      SlipPartition(j) = part_m;
      end
end

aspRad = 6e-6;
aspArea = pi*aspRad^2;

R_air = 287.1;           % gas constant for air
R_He = 2077;           % gas constant for helium
(http://www.engineeringtoolbox.com/individual-universal-gas-constant-
d\_588.html)

gam_air = 1.4;         % specific heat ratio for air
gam_He = 1.66;        % specific heat ratio for helium
(http://www.engineeringtoolbox.com/specific-heat-ratio-d\_608.html)

soundSpeedAir = sqrt(gam_air*R_air*Tinit);
soundSpeedHe = sqrt(gam_He*R_He*Tinit);

L_VM300 = 272e3;      % Latent heat of fusion (J/kg) [Iron:
http://www.engineeringtoolbox.com/fusion-heat-metals-d\_1266.html]

h=100;               % surface convection
% Tf=293;           % surface temperture (K)
Tf=1000;             % air temperture (K)

force_data= (DADS_Jan2008_noheader_alldata_refined(:,46) +
DADS_Jan2008_noheader_alldata_refined(:,47))*4.448;
% contact force between bottom of
slipper/top of rail (Newtons)

P = force_data/(An*slideCont);           % pressure (Pa N/m^2)
PV = (P*10^-6).*(vsled_horiz*1000);      % used to find montgomery's COF

COF = zeros(length(PV),1);

for index = 1:length(COF)
    if PV(index) < 4.45e8
        COF(index) = 0.2696*exp(-3.409e-7*PV(index))+0.3074*exp(-6.08e-
9*PV(index));
    else
        COF(index) = 0.02;
    end
end

% Calculate Frictional Heating (Heat Flux)

```

```

% f = 6.4969e+004;
% g = 0.6720;
% FrictHeat = f*exp(g*time);

% HeatFlux = SlipPartition .* FrictHeat/An;
HeatFlux=SlipPartition.*P.*vsled_horiz.*COF;          % (Watts/m^2)
% HeatFlux=SlipPartition'.*P.*max(vsled_horiz)/2.*COF;          %
(Watts/m^2) %Linear acceleration
% HeatFlux=SlipPartition.*P.*max(vsled_horiz).*COF;          % (Watts/m^2)
%Constant max velocity

% Calculate Temperature Profiles Using Finite Difference Method
% spatial discretization
M = 100; %number of spatial steps
dxi = 1/M;
xi = (0:dxi:1);
ystar = sqrt(alpha*time(end));

% On/Off switch for boundary condition
m = sign(force_data);
m=ones(40701,1);
% temporal discretization
N = length(time); %number of time steps
dt = time(2)- time(1);

%value initialization
v_xi_t = zeros(length(xi),N);
sigma = zeros(1,N);
sigmadot = zeros(1,N);
g_t = zeros(length(xi),N);
% g_t(1,1:2) =(2*dt*alpha)/(ystar*dxi*Km*(Tmelt-
Tinit))*(m(1:2).*(HeatFlux(1:2))+(1-m(1:2))*(Tf-Tinit)*h);
g_t(1,1:2) =(2*dt*alpha)/(ystar*dxi*Km*(Tmelt-
Tinit))*(m(1:2).*(HeatFlux(1:2))+(1-m(1:2))*(Tf-Tinit)*h);
d = [-1; 0; 1];

%calculations based on explicit solution
v_xi_t(:,2) = g_t(:,1);
r = waitbar(0, 'Please wait...');
for tn = 2:N-1
    dt = time(tn+1) - time(tn);
    B1(:,1) = [(alpha*dt/(ystar^2*dxi^2) -
dt/(2*ystar*dxi)*sigmadot(tn))*ones(length(xi)-1,1);0];
    B1(:,2) = [1-dt*(2*alpha/(ystar*dxi)^2+(2*alpha/(ystar*dxi)^2-
sigmadot(tn)/(2*ystar*dxi))*((2*dxi*ystar*(1-m(tn)))/Km)*h);(1 -
2*alpha*dt/(ystar^2*dxi^2))*ones(length(xi)-1,1)];
    B1(:,3) = [0; 2*alpha*dt/(ystar^2*dxi^2); (alpha*dt/(ystar^2*dxi^2)
+ dt/(2*ystar*dxi)*sigmadot(tn))*ones(length(xi)-2,1)];
    B = spdiags(B1,d,length(xi),length(xi));
    clear B1
    v_xi_t(:,tn+1) = B*v_xi_t(:,tn) + g_t(:,tn);
    clear B

    I = find(v_xi_t(:,tn+1)>1);

```

```

chk = 1;
while ~isempty(I)
    if chk == 1
        delsig = .01*interp1(v_xi_t(:,tn+1),xi,1,'linear');
        chk = 2;
    end
    sigma(tn) = sigma(tn) + ystar*delsig;
    sigmadot(tn) = (sigma(tn) - sigma(tn-1))/dt;
    B1(:,1) = [(alpha*dt/(ystar^2*dxi^2) -
dt/(2*ystar*dxi)*sigmadot(tn))*ones(length(xi)-1,1);0];
    B1(:,2) = [1-dt*(2*alpha/(ystar*dxi)^2+(2*alpha/(ystar*dxi)^2-
sigmadot(tn)/(2*ystar*dxi))*((2*dxi*ystar*(1-m(tn))/Km)*h);(1 -
2*alpha*dt/(ystar^2*dxi^2))*ones(length(xi)-1,1)];
    B1(:,3) = [0; 2*alpha*dt/(ystar^2*dxi^2); (alpha*dt/(ystar^2*dxi^2)
+ dt/(2*ystar*dxi)*sigmadot(tn))*ones(length(xi)-2,1)];
    B = spdiags(B1,d,length(xi),length(xi));
    clear B1
    g_t(1,tn) = dt/(Km*(Tinit-Tmelt))*(sigmadot(tn)-
2*alpha/(ystar*dxi))*(m(tn).*(HeatFlux(tn) -
rho_V300*L_VM300*sigmadot(tn)))+(1-m(tn))*(Tf-Tinit)*h);
    v_xi_t(:,tn+1) = B*v_xi_t(:,tn) + g_t(:,tn);
    clear I B
    I = find(v_xi_t(:,tn+1)>1);
end
sigma(tn+1:end) = sigma(tn);
g_t(1,tn+1) = (2*dt*alpha)/(ystar*dxi*Km*(Tmelt-
Tinit))*(m(tn+1).*(HeatFlux(tn+1)))+(1-m(tn+1))*(Tf-Tinit)*h);
waitbar((tn-1)/(N-2),r)
end
close(r);

%%
[T,TotalMeltWear]=plots(Tmelt, Tinit, v_xi_t, time, SlipPartition);

%% Plots function
function [T,TotalMeltWear]=plots(Tmelt, Tinit, v_xi_t, time,
SlipPartition)
global Tmelt Tinit v_xi_t time sigma thickness SlipPartition melt_wear
cg_horiz

hold on
figure(1)
plot(time,SlipPartition,'r') % analytical heat partition solution
plot(time,SlipPartition,'r') % hypothesized heat partition function
title('Heat partition into Slipper vs Sliding time','fontsize',14)
xlabel('Sliding Time(sec)','fontsize',10)
ylabel('Heat Partition','fontsize',10)

% Make a graph of sliding time vs temperature at surface
T = (Tmelt - Tinit)*v_xi_t + Tinit;
hold on
figure(2)
subplot(2,1,1); plot(time,T,'r')
title('Surface Temperature vs Sliding time','fontsize',14)
xlabel('Sliding Time (sec)','fontsize',10)

```

```

ylabel('Surface Temperature','fontsize',10)

% Make a graph of sliding time vs percentage of shoe thickness melted
T = (Tmelt - Tinit)*v_xi_t + Tinit;
hold on
figure(2)
melt_wear=(sigma/thickness*100);
subplot(2,1,2); plot(time,melt_wear,'r:')
title('Percentage of shoe thickness melted vs Sliding
time','fontsize',14)
xlabel('Sliding time (sec)','fontsize',10)
ylabel('Percentage of Shoe Thickness Melted','fontsize',10)

figure(3)
subplot(2,1,1); plot(cg_horiz',melt_wear)
title('Percentage of shoe thickness melted vs Sliding
distance','fontsize',14)
xlabel('Sliding distance (m)','fontsize',10)
ylabel('Percentage of Shoe Thickness Melted','fontsize',10)

subplot(2,1,2); plot(cg_horiz',sigma)

TotalMeltWear=melt_wear(end);

```

## Bibliography

1. Buentello, R. G. *3D Finite Element Modeling of Sliding Wear*. Ph. D. prospectus, Air Force Institute of Technology, Wright-Patterson AFB, OH, 2013.
2. Hale, C. S. *Consideration of Wear Rates at High Velocity AFIT/DS/ENY/10-08*. Ph. D. dissertation, Air Force Institute of Technology, Wright-Patterson AFB, OH, 2010.
3. Johnson, G. R. and W. H. Cook. "A Constitutive Model and Data for Metals Subjected to Large Strains, High Strain Rates and High Temperatures." Proceedings of the 7th International Symposium on Ballistics. April 1983.
4. Korkegi, R. H. and R. A. Briggs. "The Hypersonic Slipper Bearing - A Test Track Problem," *Journal of Spacecraft & Rockets*, 6(2):210–212, 1969.
5. Krupovage, D. J. and H. J. Rassmussen. Hypersonic Rocket Sled Development. Technical Report AD-TR-82-41, Test Track Division, 6585th Test Group, Holloman AFB, New Mexico, September 1981.
6. Laird, D. J. *The Investigation of Hypervelocity Gouging AFIT/DS/ENY/02-01*. Ph. D. dissertation, Air Force Institute of Technology, Wright-Patterson AFB, OH, 2002.
7. Laird, D. J. and A. N. Palazotto. "Effect of Temperature on the Process of Hypervelocity Gouging," *AIAA Journal*, 41(11):2251–2260, 2003.
8. Meador, S. P. *Consideration of Wear at High Velocities AFIT/GAE/ENY/10-M16*. Master's thesis, Air Force Institute of Technology, Wright-Patterson AFB, OH 2010.
9. Montgomery, R. S. "Friction and Wear at High Sliding Speeds," *Wear*, 36(3):275–298, March 1976.
10. Moran, M. J., H. N. Shapiro, and D. P. DeWitt. *Introduction to Thermal Systems Engineering*. John Wiley and Sons, Inc., New Jersey, 2003.

11. Paek-Spidell, G. *Analysis of Heat Partition Fractions in Sliding Contact at High Speeds and High Pressures and Its Effects on Materials*. Ph. D. prospectus, Air Force Institute of Technology, Wright-Patterson AFB, OH 2012.
12. Wolfson, M. R. *Wear, Solid Lubrication, and Bearing Material Investigation for High-Speed Track Applications*. Technical Report AFMDC-TR-60-7, Test Track Division, Air Force Missile Development Center, Holloman AFB, New Mexico, March 1960.

## REPORT DOCUMENTATION PAGE

*Form Approved*  
*OMB No. 074-0188*

The public reporting burden for this collection of information is estimated to average 1 hour per response, including the time for reviewing instructions, searching existing data sources, gathering and maintaining the data needed, and completing and reviewing the collection of information. Send comments regarding this burden estimate or any other aspect of the collection of information, including suggestions for reducing this burden to Department of Defense, Washington Headquarters Services, Directorate for Information Operations and Reports (0704-0188), 1215 Jefferson Davis Highway, Suite 1204, Arlington, VA 22202-4302. Respondents should be aware that notwithstanding any other provision of law, no person shall be subject to any penalty for failing to comply with a collection of information if it does not display a currently valid OMB control number.

**PLEASE DO NOT RETURN YOUR FORM TO THE ABOVE ADDRESS.**

<b>1. REPORT DATE</b> (DD-MM-YYYY) 21-03-2013			<b>2. REPORT TYPE</b> Master's Thesis		<b>3. DATES COVERED</b> (From - To) 1 Aug 11 - 21 Mar 13	
<b>4. TITLE AND SUBTITLE</b> A Study of the Thermal Environment Developed by a Traveling Slipper at High Velocity				<b>5a. CONTRACT NUMBER</b>		
				<b>5b. GRANT NUMBER</b>		
				<b>5c. PROGRAM ELEMENT NUMBER</b>		
<b>6. AUTHOR(S)</b> Le, Kathleen H., Captain, USAF				<b>5d. PROJECT NUMBER</b> N/A		
				<b>5e. TASK NUMBER</b>		
				<b>5f. WORK UNIT NUMBER</b>		
<b>7. PERFORMING ORGANIZATION NAMES(S) AND ADDRESS(S)</b> Air Force Institute of Technology Graduate School of Engineering and Management (AFIT/EN) 2950 Hobson Way, Building 640 WPAFB OH 45433				<b>8. PERFORMING ORGANIZATION REPORT NUMBER</b>  AFIT-ENY-13-M-20		
<b>9. SPONSORING/MONITORING AGENCY NAME(S) AND ADDRESS(ES)</b> Intentionally left blank				<b>10. SPONSOR/MONITOR'S ACRONYM(S)</b>		
				<b>11. SPONSOR/MONITOR'S REPORT NUMBER(S)</b>		
<b>12. DISTRIBUTION/AVAILABILITY STATEMENT</b> Approved for Public Release; Distribution Unlimited.						
<b>13. SUPPLEMENTARY NOTES</b>						
<b>14. ABSTRACT</b> The research presented in this thesis is developed from the relative sliding motion of a traveling slipper and stationary rail at the Holloman High Speed Test Track located at Holloman AFB, NM. The high velocity condition of the slipper traveling down the rail creates a thermal environment that is of interest to the researchers at the Air Force Institute of Technology. The high temperatures coupled with high velocity leads to a non-linear problem known as melt wear. The goal of this research is to characterize the amount of heat flow going into the slipper as it traverses the rail and to predict the total melt wear of the slipper.						
<b>15. SUBJECT TERMS</b> Holloman High Speed Test Track, melt wear						
<b>16. SECURITY CLASSIFICATION OF:</b>			<b>17. LIMITATION OF ABSTRACT</b>	<b>18. NUMBER OF PAGES</b>	<b>19a. NAME OF RESPONSIBLE PERSON</b> Anthony N. Palazotto (ENY)	
<b>a. REPORT</b>	<b>b. ABSTRACT</b>	<b>c. THIS PAGE</b>			<b>19b. TELEPHONE NUMBER</b> (Include area code) (937) 255-6565 x4599, (anthony.palazotto@afit.edu)	
U	U	U	UU	82		